

Large scale industrial and geophysical flow modelling

Paul Cleary

CSIRO Mathematical and Information Sciences

Overview

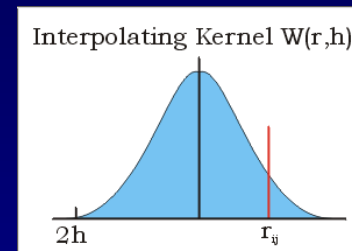
- SPH details for fluids, elastoplastic and elastic-brittle models
- Strengths of SPH for industrial and geophysical modelling
- Manufacturing processes
- Mineral processing
- Pyrometallurgy
- Fracture
- Fluid-discrete particle
- Fluid-discrete bubble
- Fluid gas (using SPH-FD/FV)
- Interesting examples

SPH – Summary of Theory

Particle equations of motion are derived from the governing PDEs (such as Navier-Stokes, linear elastic solid stress equations) using a spatial smoothing or interpolation process:

$$A(\mathbf{r}) = \sum_b m_b \frac{A_b}{\rho_b} W(\mathbf{r} - \mathbf{r}_b, h)$$

$$\nabla A(\mathbf{r}) = \sum_b m_b \frac{A_b}{\rho_b} \nabla W(\mathbf{r} - \mathbf{r}_b, h)$$



Continuity Equation

$$\frac{d\rho_a}{dt} = \sum_b m_b (\mathbf{v}_a - \mathbf{v}_b) \cdot \nabla W_{ab}$$

Momentum Equation

$$\frac{d\mathbf{v}_a}{dt} = \mathbf{g} - \sum_b m_b \left[\left(\frac{P_b}{\rho_b^2} + \frac{P_a}{\rho_a^2} \right) - \frac{\xi}{\rho_a \rho_b (\mu_a + \mu_b)} \frac{\mathbf{v}_{ab} \cdot \mathbf{r}_{ab}}{r_{ab}^2 + \eta^2} \right] \nabla_a W_{ab}$$

Equation of state

$$P = P_0 \left[\left(\frac{\rho}{\rho_0} \right)^{\gamma} - 1 \right] \quad \text{where} \quad \frac{\gamma P_0}{\rho_0} = c_s^2 = \alpha V^2$$

Energy Equation

$$\frac{dH_a}{dt} = \sum_b \frac{4m_b}{\rho_a \rho_b} \frac{k_a k_b}{k_a + k_b} T_{ab} \frac{\mathbf{r}_{ab} \cdot \nabla_a W_{ab}}{r_{ab}^2 + \eta^2}$$

$$\text{Enthalpy } H = \int_0^T c_p(\theta) d\theta + L[1 - f_s(T)]$$

Solid boundaries are typically implemented using wall forces



SPH equations for solid deformation

The momentum equation for the elasto-plastic deformation of solids is:

$$\frac{dv^i}{dt} = \frac{1}{\rho_s} \frac{\partial \sigma^{ij}}{\partial x^j} + g^i$$

where v is velocity, g denotes the body force and σ is the stress tensor which can be written as:

$$\sigma^{ij} = -P_s \delta^{ij} + S^{ij}$$

where P_s is the pressure and S is the deviatoric stress. Assuming Hooke's law with shear modulus μ_s the evolution equation for S is:

$$\frac{dS^{ij}}{dt} = 2\mu_s \left(\dot{\epsilon}^{ij} - \frac{1}{3} \delta^{ij} \dot{\epsilon}^{kk} \right) + S^{ik} \Omega^{jk} + \Omega^{ik} S^{kj}$$

where $\dot{\epsilon}^{ij} = \frac{1}{2} \left(\frac{\partial v^i}{\partial x^j} + \frac{\partial v^j}{\partial x^i} \right)$ and $\Omega^{ij} = \frac{1}{2} \left(\frac{\partial v^i}{\partial x^j} - \frac{\partial v^j}{\partial x^i} \right)$ is the rotation tensor.

The equation of state $P_s = c_0^2 (\rho_s - \rho_{s0})$ and the Poisson ratio is:

$$\nu_s = \frac{(3K / \mu_s - 2)}{2(3K / \mu_s + 2)}$$

Libersky and Petschek (1990), Wingate and Fisher (1993), Gray *et al.*, (2001)



Plasticity model

Radial return plasticity model:

The trial stress S_{Tr}^{ij} is the deviatoric part of the stress calculated assuming that the initial response is elastic

$$S^{ij} = \alpha S_{Tr}^{ij}$$

where S^{ij} is the final deviatoric stress at the end of a time-step and α is a proportionality constant given by:

$$\alpha = \left(1 - \frac{3\mu_s \Delta \bar{\epsilon}^p}{\bar{\sigma}^{Tr}} \right)$$

$\sqrt{\frac{2}{3}} \bar{\sigma}^{Tr}$ is the magnitude of the trial deviatoric stress and $\Delta \bar{\epsilon}^p$ is the increment in equivalent plastic strain:

$$\Delta \bar{\epsilon}^p = \frac{\bar{\sigma}^{Tr} - \sigma_y^n}{3\mu_s + H}$$

where σ_y^n is the final yield stress and H is the hardening modulus.

The stress update is completed by adding the deviatoric and mean stress.

The plastic strain is incremented as: $\bar{\epsilon}^p = \bar{\epsilon}^p + \Delta \bar{\epsilon}^p$

Brittle Fracture

- Brittle fracture plays an important role in many industrial processes (oil/gas recovery, mining, casting, extrusion, impact etc), failures in industrial components and geophysical events
- A modified form of the Grady-Kipp damage model has been developed
- This model is useful for the prediction of rock damage (volume averaged cracking of rock) based on local stress history and flaw distribution
- Approximate differential form for damage $D(t)$ evolution is:

$$\frac{dD^{1/3}}{dt} = \frac{(m+3)}{3} \alpha^{1/3} \epsilon^{m/3} \quad \text{and} \quad \alpha = \frac{8\pi C_g^3 k}{(m+1)(m+2)(m+3)}$$

- Using closure for the strain by Melosh et al (1992)

$$\epsilon_{eff} = \sigma_{max} / \left(K + \frac{4}{3} G \right)$$

- Damage accumulates when strain exceeds a threshold ϵ_{min}

The *strengths* of SPH

- Free surfaces (including waves, splashing and fragmentation) are handled easily and naturally, without mass loss to give accurate representations of the material surface behaviour even at low resolution
- Extreme deformations of materials are easily simulated because there is no grid/mesh structure to distort and costly re-meshing is not needed
- Powerful ability to accurately represent moving objects interacting with materials (avoids the problems of alignment of object boundaries with meshes in immersed boundary methods) or of large mesh deformation (if meshes are attached to object surfaces)
- Advection is automatic and zero cost. For high speed flows, it does not create artificial numerical diffusion, does not require upwinding and since the associated non-linear convection term is omitted, solutions are more accurate and stable.

The *strengths* of SPH

- Compressible and Incompressible flows can be simulated
- Fully transient
- Complex additional physics can be added easily (e.g. solidification, freezing, non-Newtonian rheology, fabric, membranes, particulates, bubbles, solid stress ...)
- History dependence of material is simple since particles represent the same piece of material and this is automatically carried along (material type and composition, oxide level, microstructure, accumulated defects)
- Very complex geometries can be handled. Do not need high quality volume meshes through which material is to flow.

These attributes make the method ideally suited for simulating a broad range of fluid flow and solid deformation processes



Filling of a glass



SPH predicts surface wave motion and surface breakup



Filling of a glass with milk



Complex surface splashing as waves converge from the sides

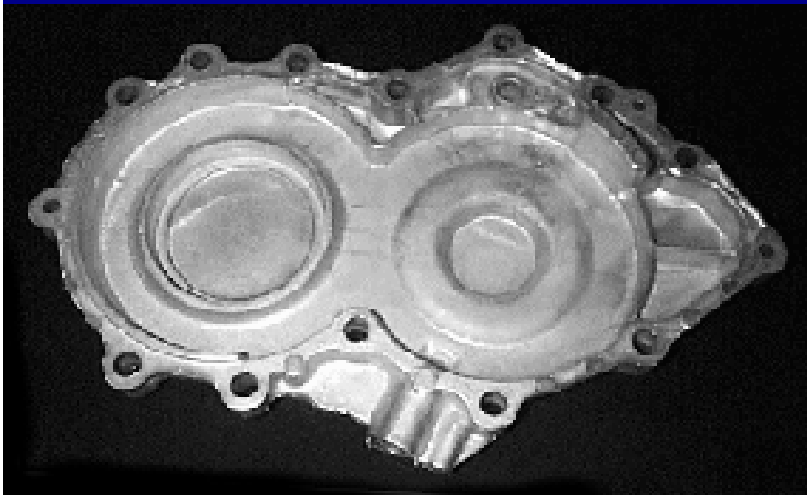
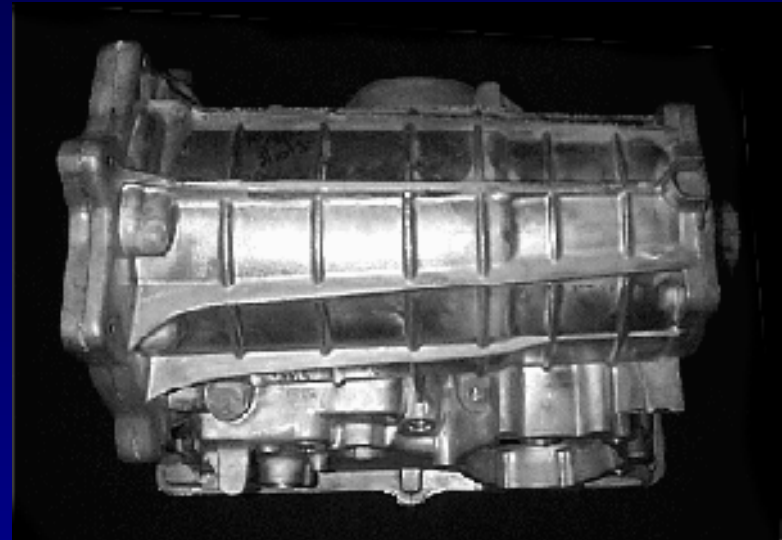
Manufacturing Processes

High Pressure Die Casting

Liquid metal is injected at speeds of 30-100 m/s under high pressure:

- Flows are fast and complex
- Free surface behaviour is extremely complex with fragmentation and droplet formation

The process is not well understood

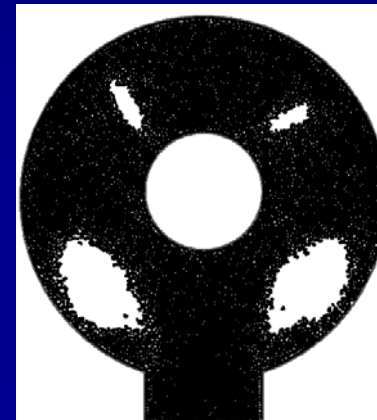
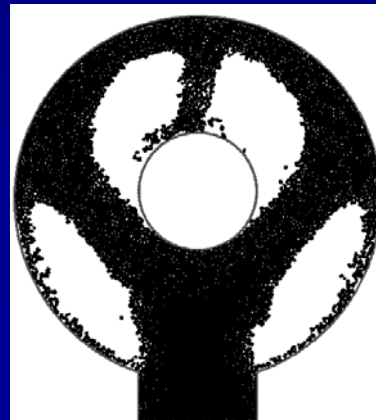
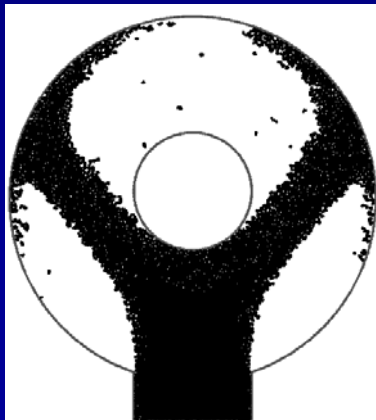


HPDC is used extensively in automotive and other industries to fabricate complex components from aluminium and potentially from magnesium

Validation: Filling annular die



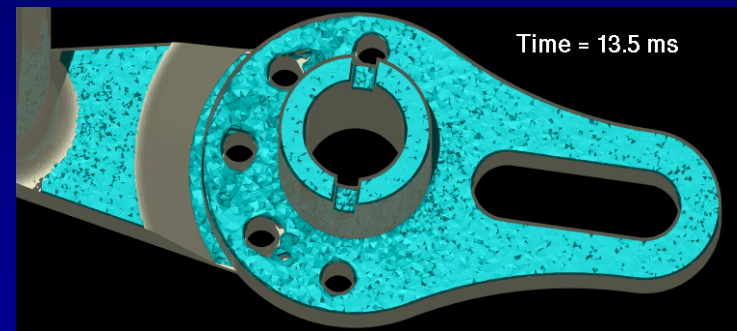
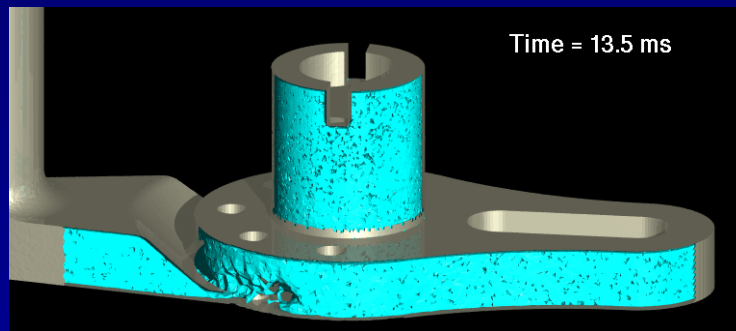
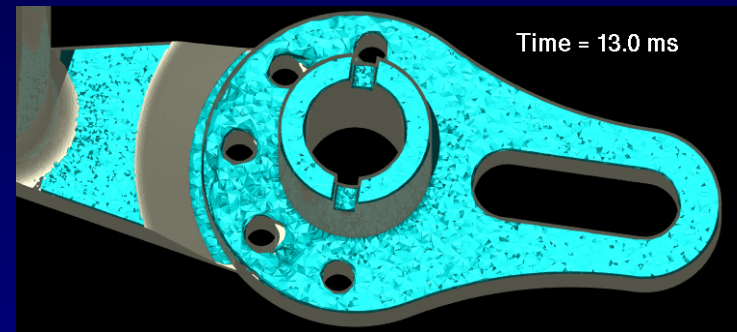
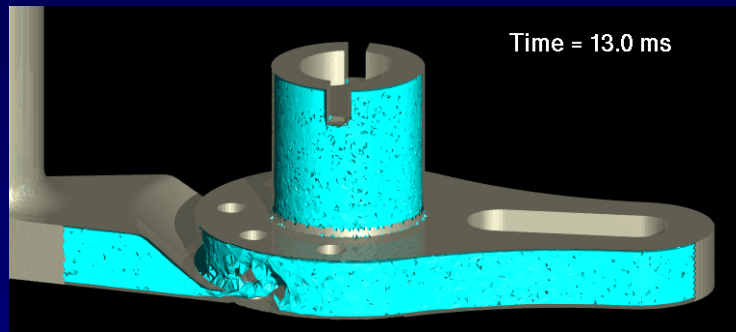
Water analogue
Experiment:
Schmidt & Klein



SPH

Effect of Reynolds Number

Top: $Re = 2700$

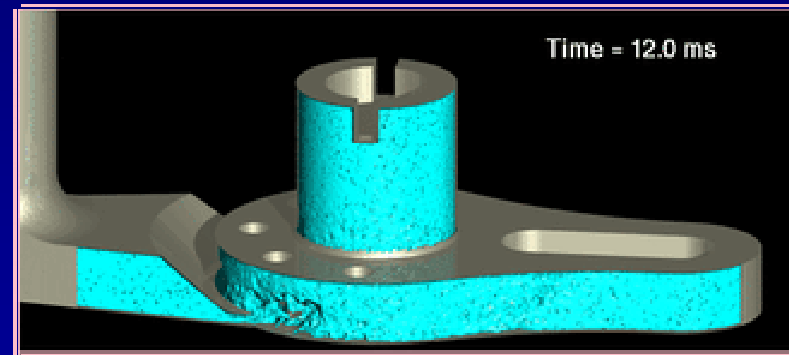
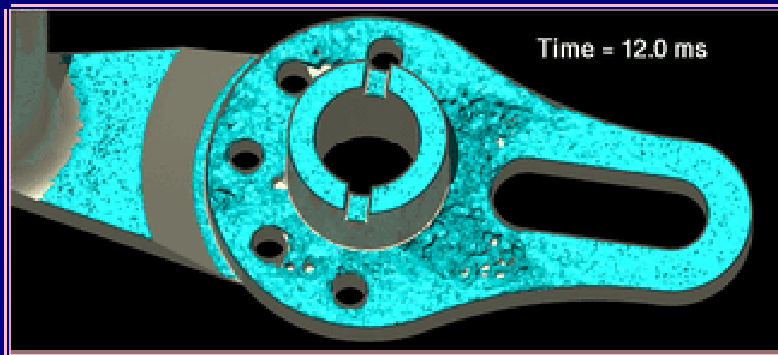
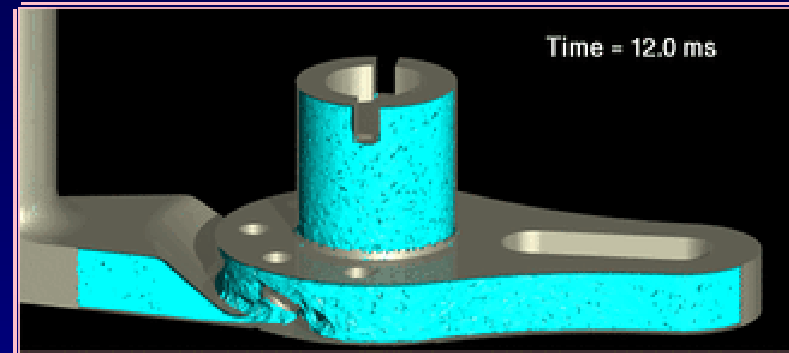
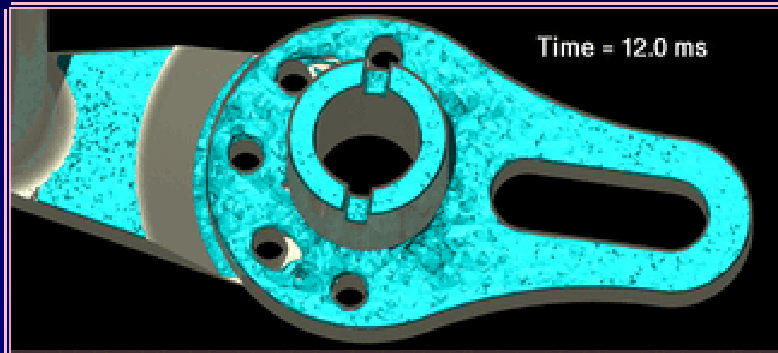


Bottom: $Re = 500$

The filling is very similar, with the higher viscosity leading to a modestly longer filling time due to increased resistance to flow through the gate

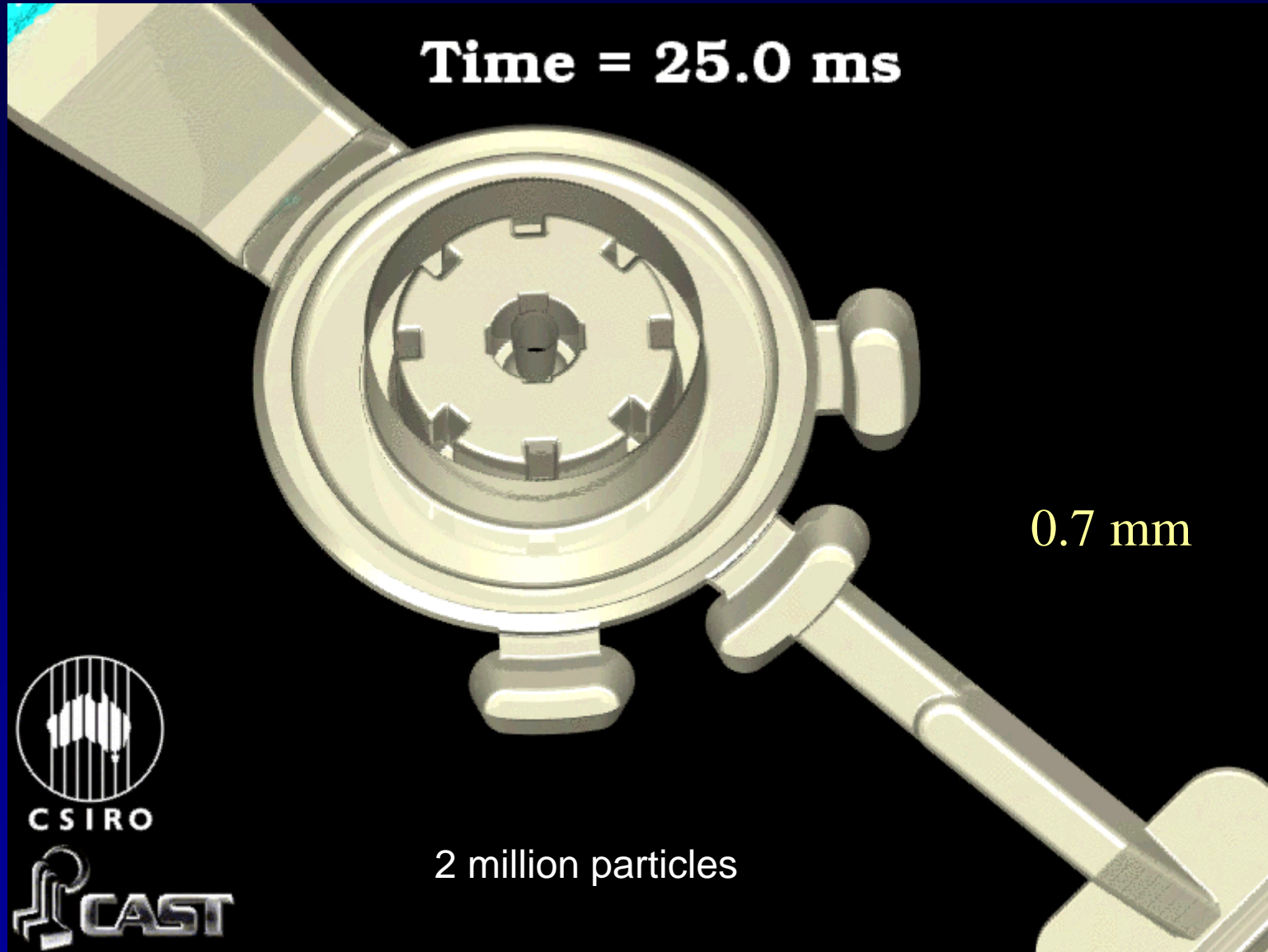
Effect of Resolution

Top: low resolution (1 particle / 1.1 mm), 370,000 particles



Bottom: high resolution (1 particle / 0.83 mm), 640,000 particles

Very close agreement is achieved for the two resolutions



Front servo piston filling



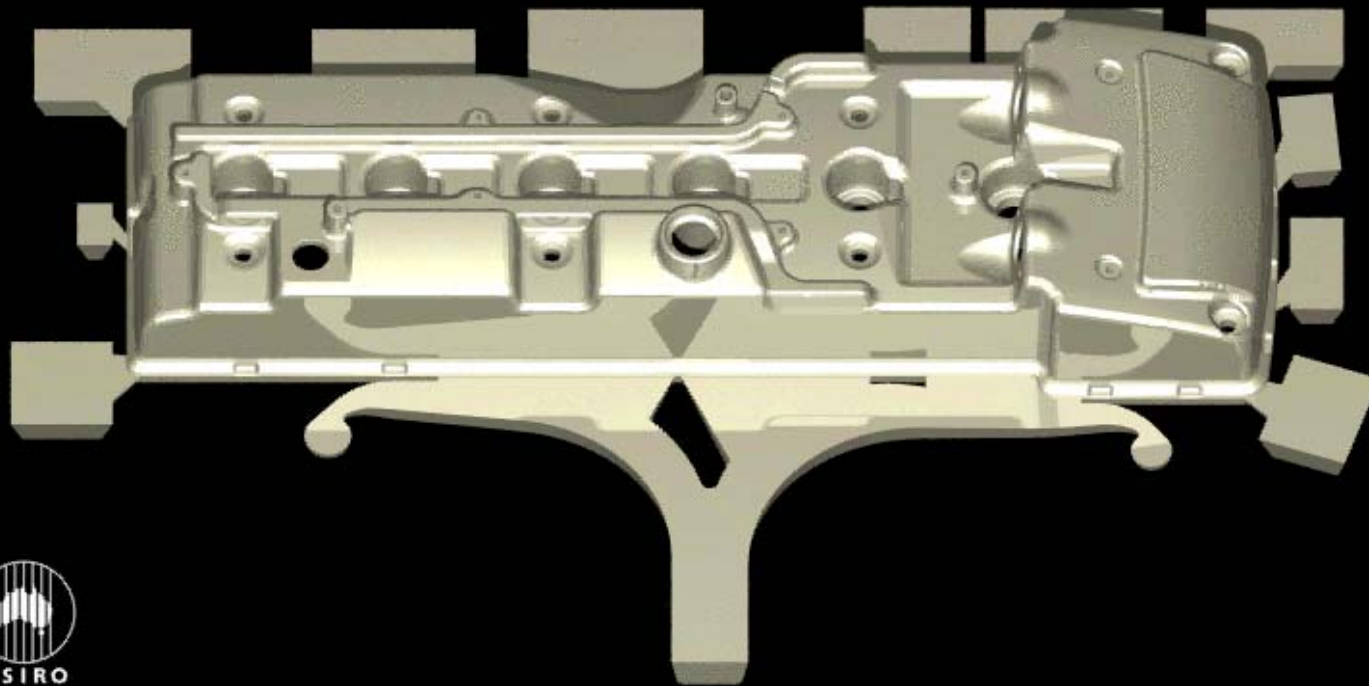
HPDC - Rocker Cover

Geometrically large and complex with thin walls makes a large problem

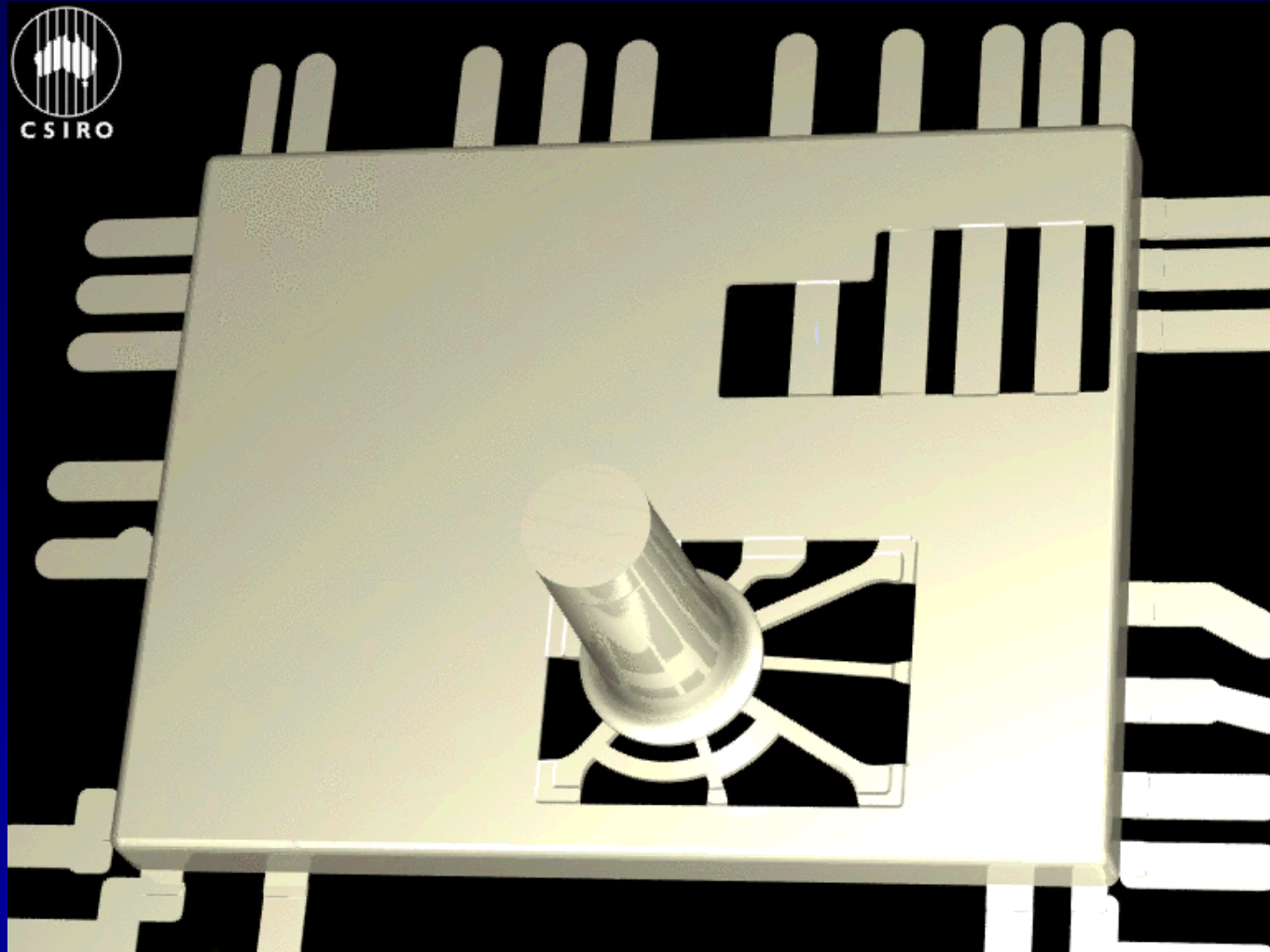
Gate 2.6 mm, wall thickness 3 mm, resolution 1.7 mm

Gate speed 12 m/s

resolution 1.25 mm



Magnesium HPDC of a laptop

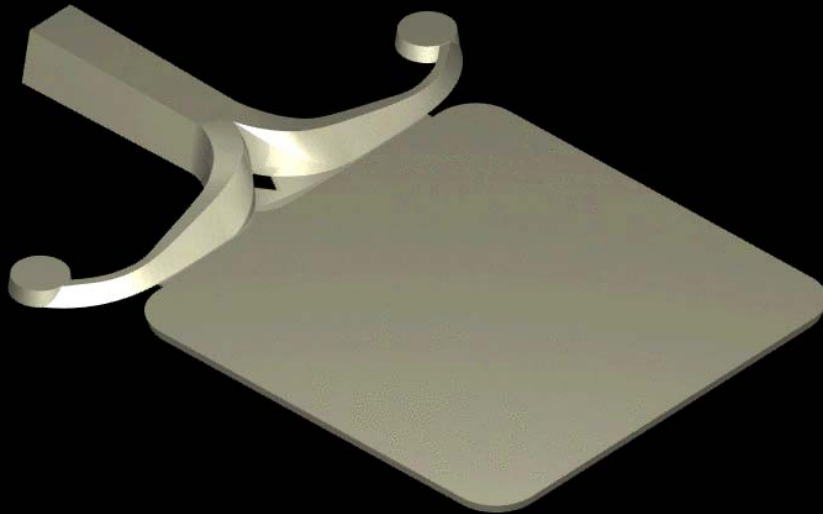


Coaster as a test case

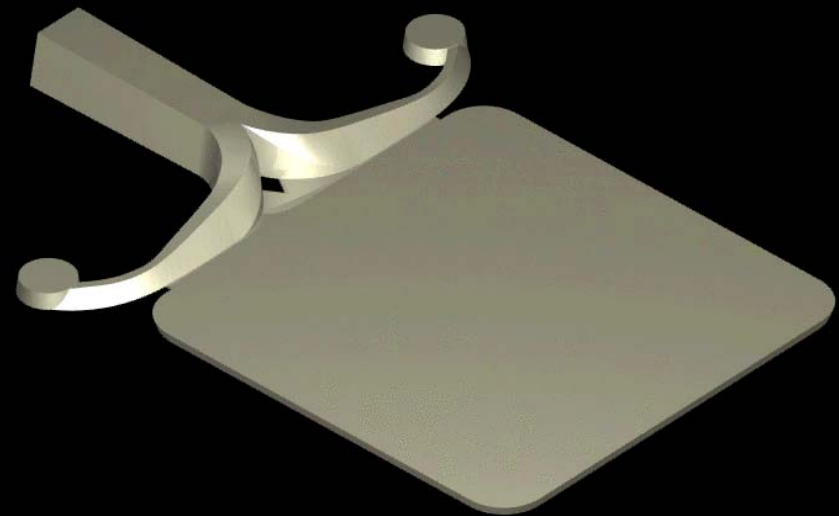
Liquid Al temperature at inflow is
+10 C superheat

Die has initial temperature of 200 C

Coupled thermal and flow



Isothermal



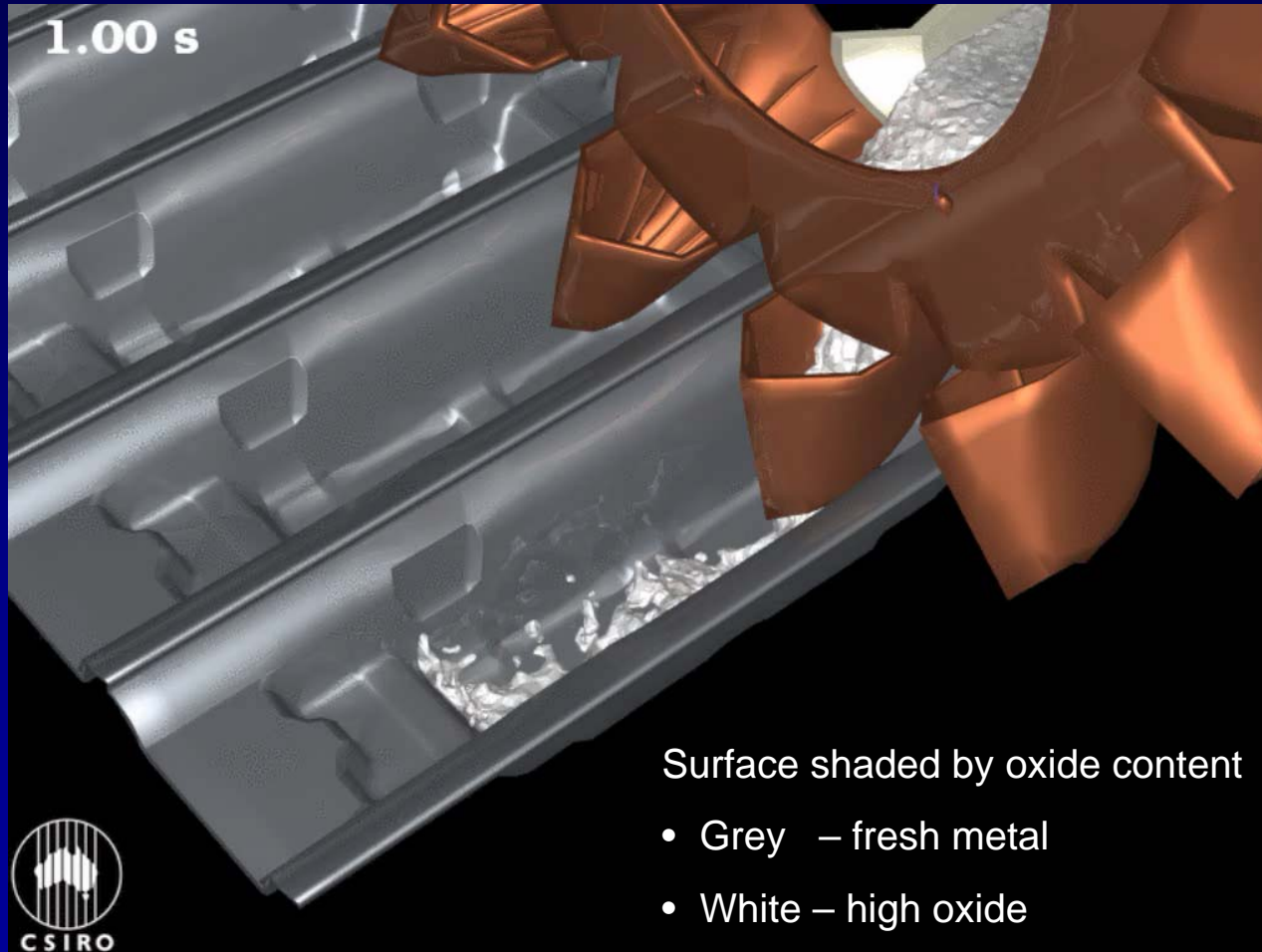
Primary metal casting – Al ingot casting

Process by which molten aluminium from smelter pot lines is turned into solid ingots for transport and sale

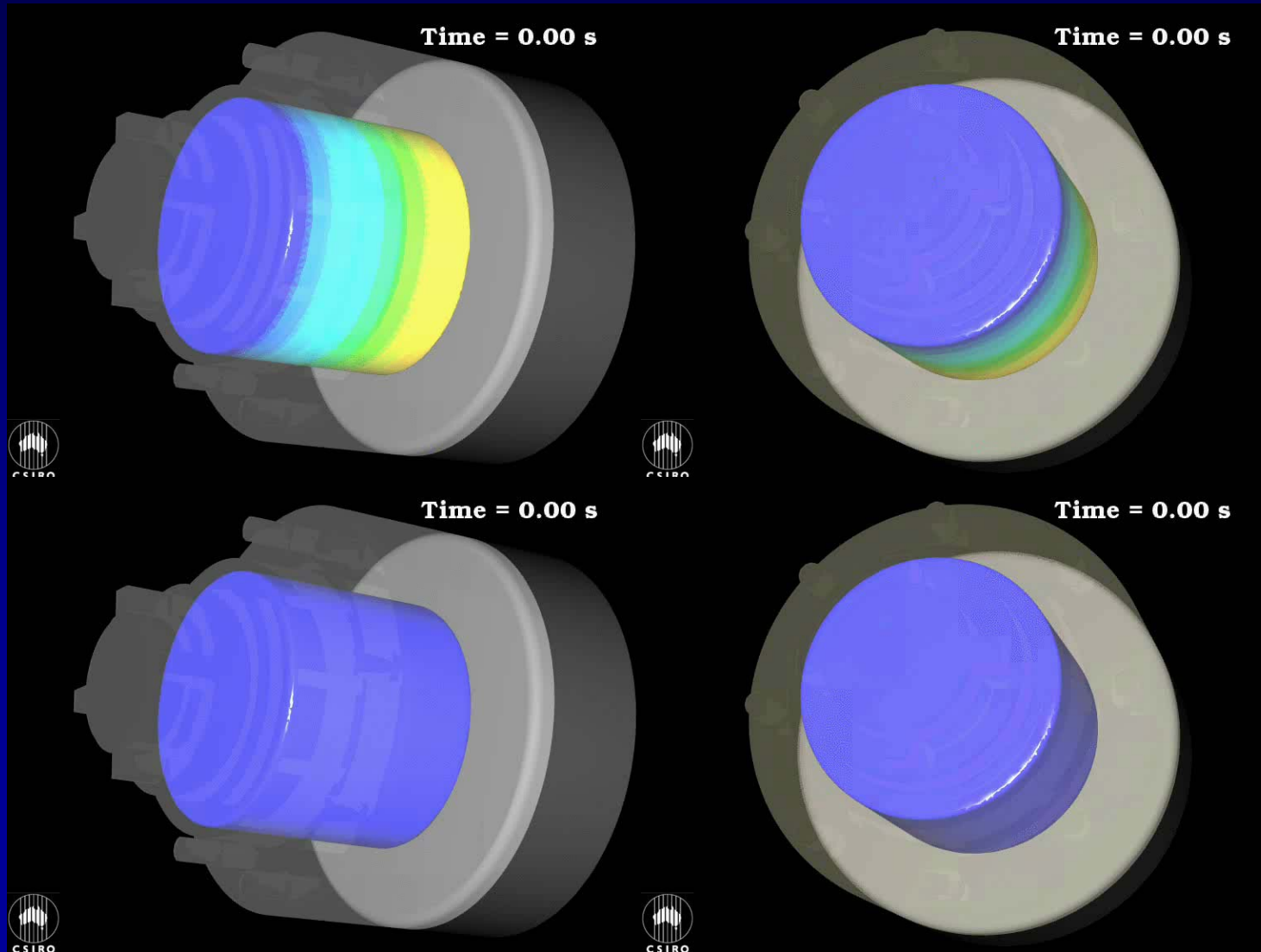


A line of moulds passes under a rotating wheel that distributes molten Al through nozzles and which is feed via a launder from a furnace

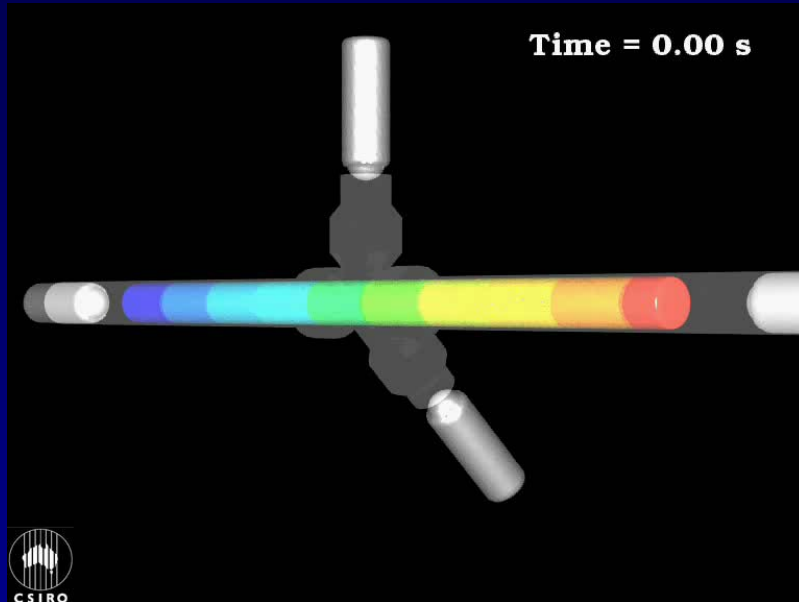
Al ingot casting – New design



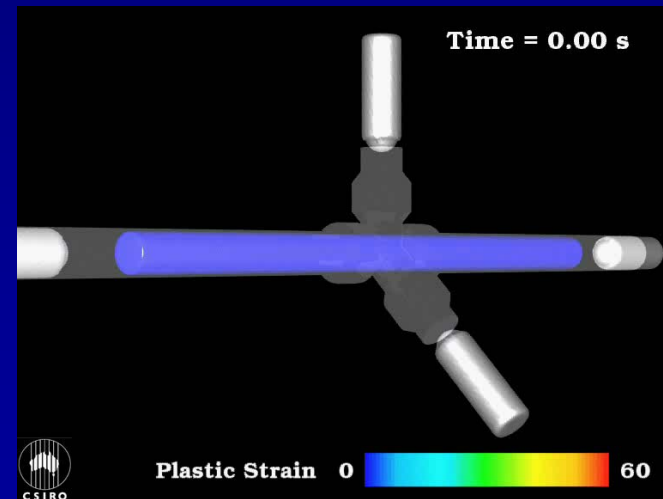
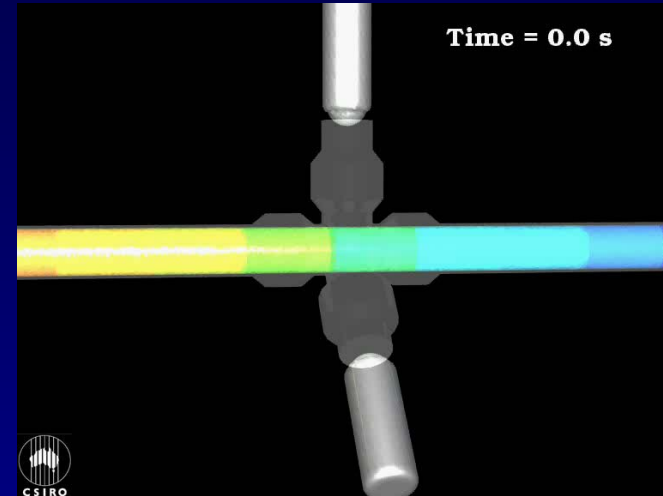
Simple 3D Forging



Multi-die Forging

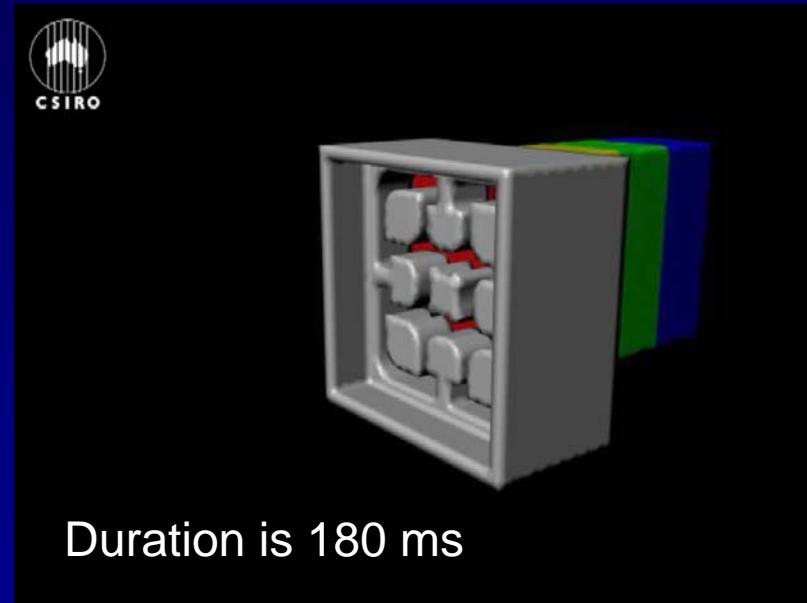
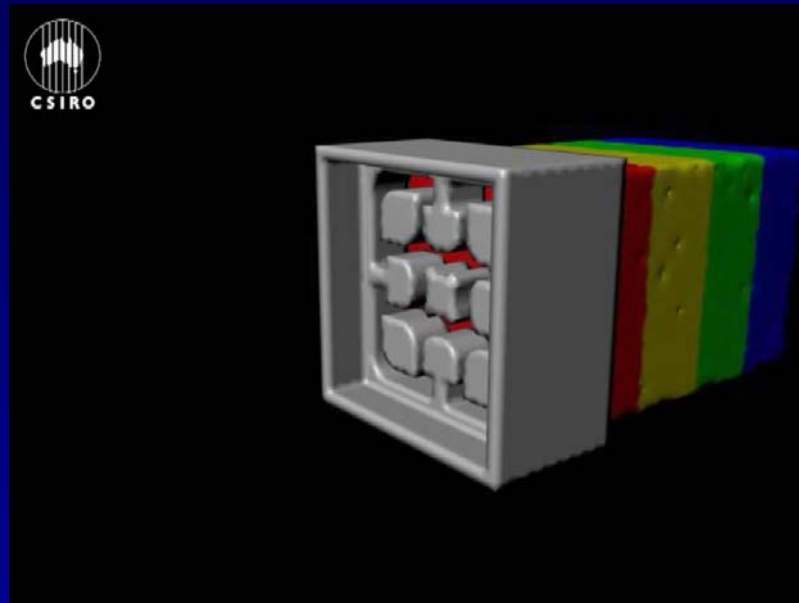


Cylindrical work piece with dies located at each end and at 120° apart in the orthogonal plan



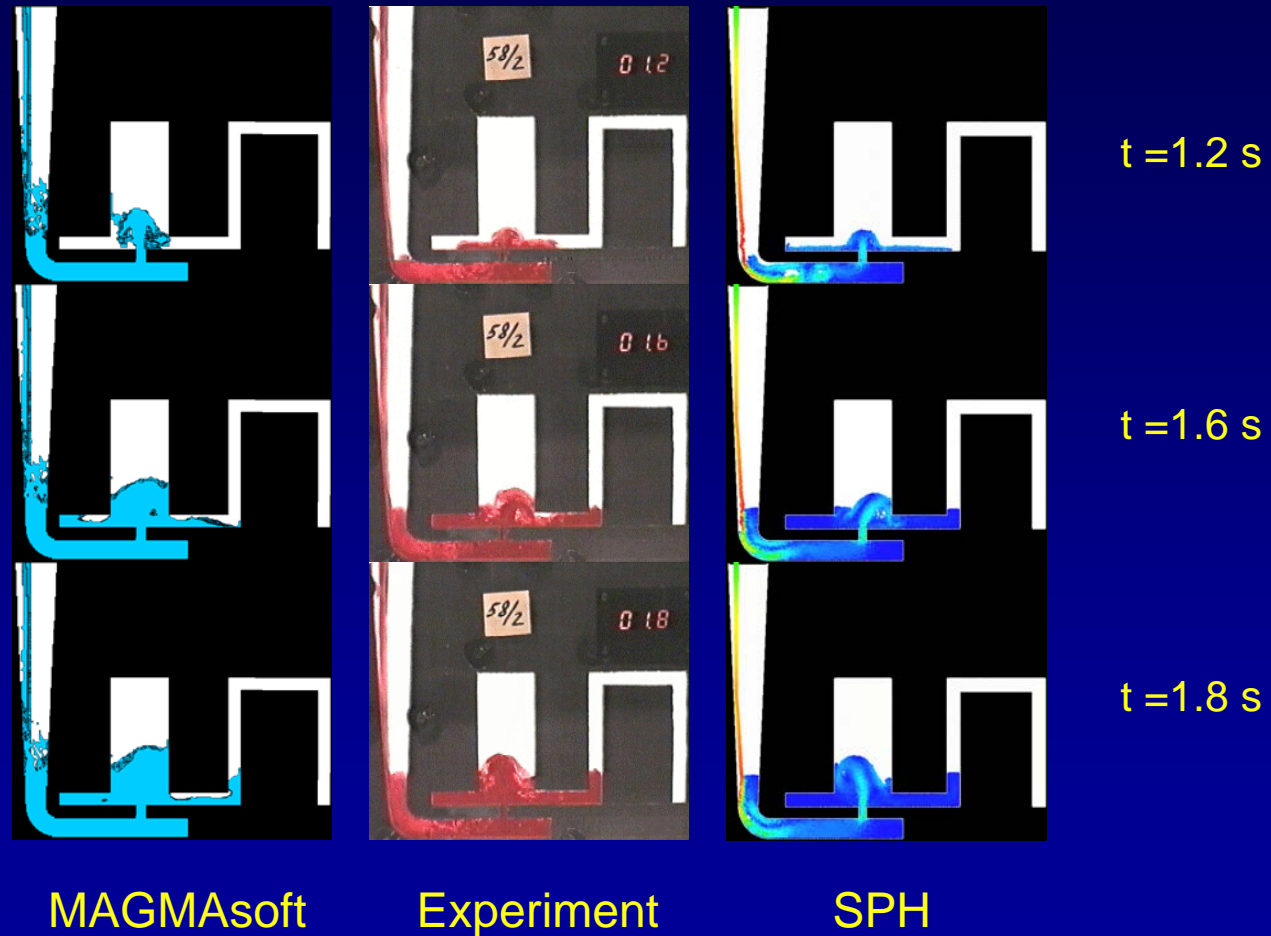
Metal deformation during extrusion

The feed metal is coloured in four bands to show the extent of deformation

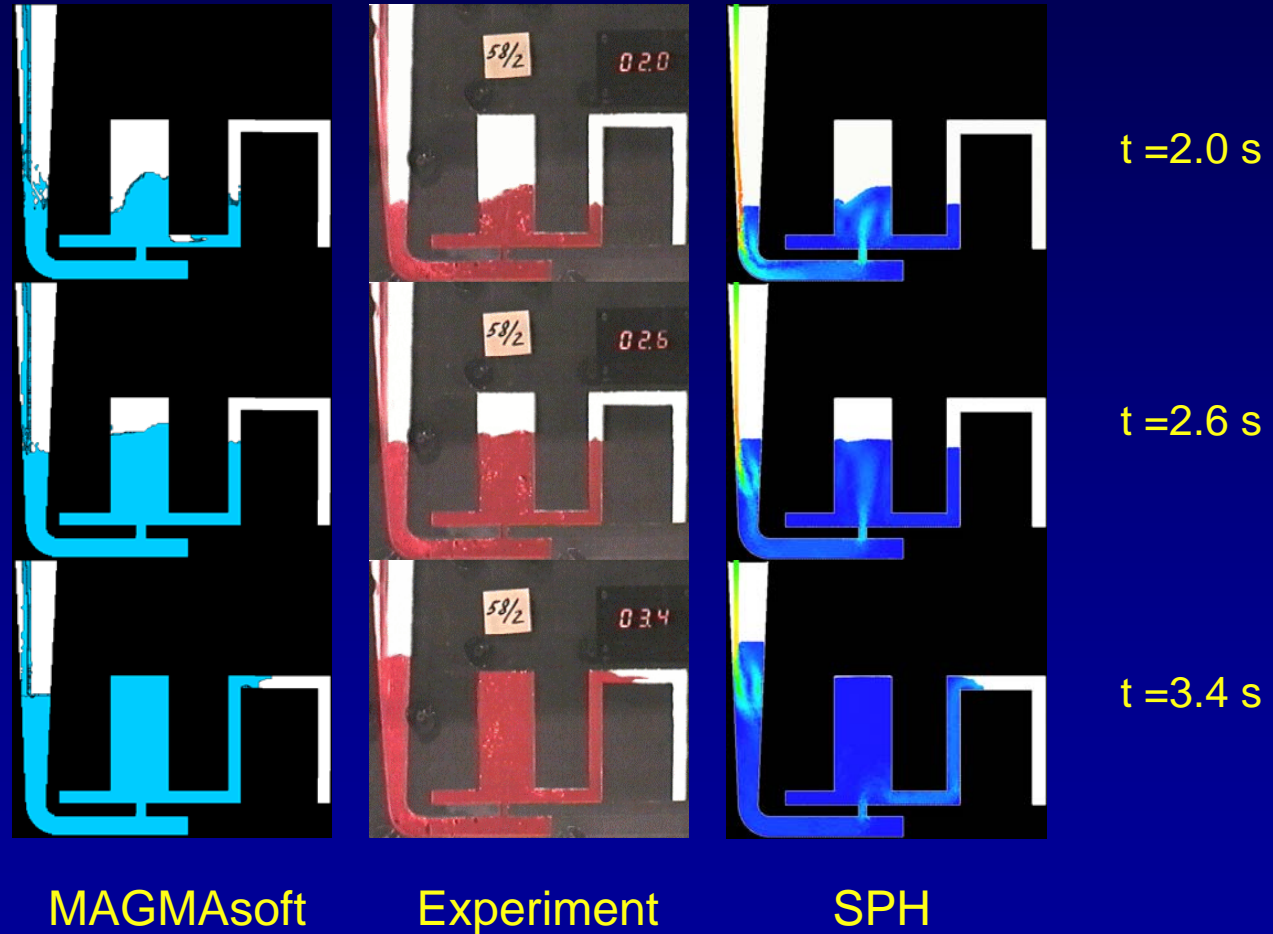


The metal elongates in the flow direction as the wider billet is forced through the narrower die opening. There is little mixing of metal between colour layers except for red material trapped in the edge regions of the die entry. This metal is progressively deposited onto the yellow material in thin surface patches

GDC validation: Horizontal Orientation

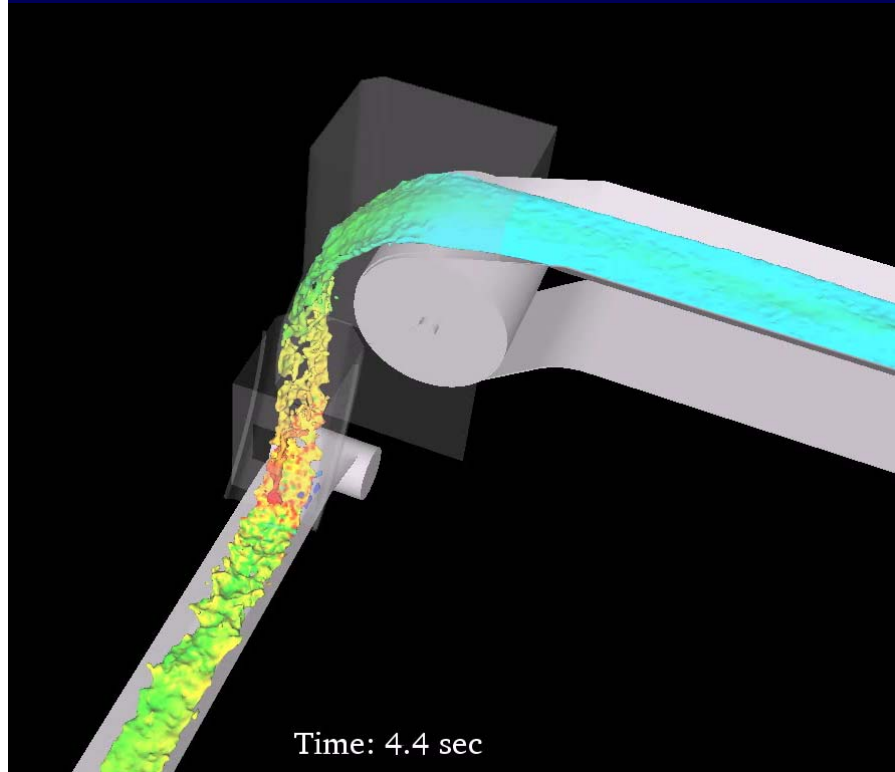


GDC validation: Horizontal Orientation



Mineral Processing

SPH model of conveyor transfer chute for slurry/fine particulates

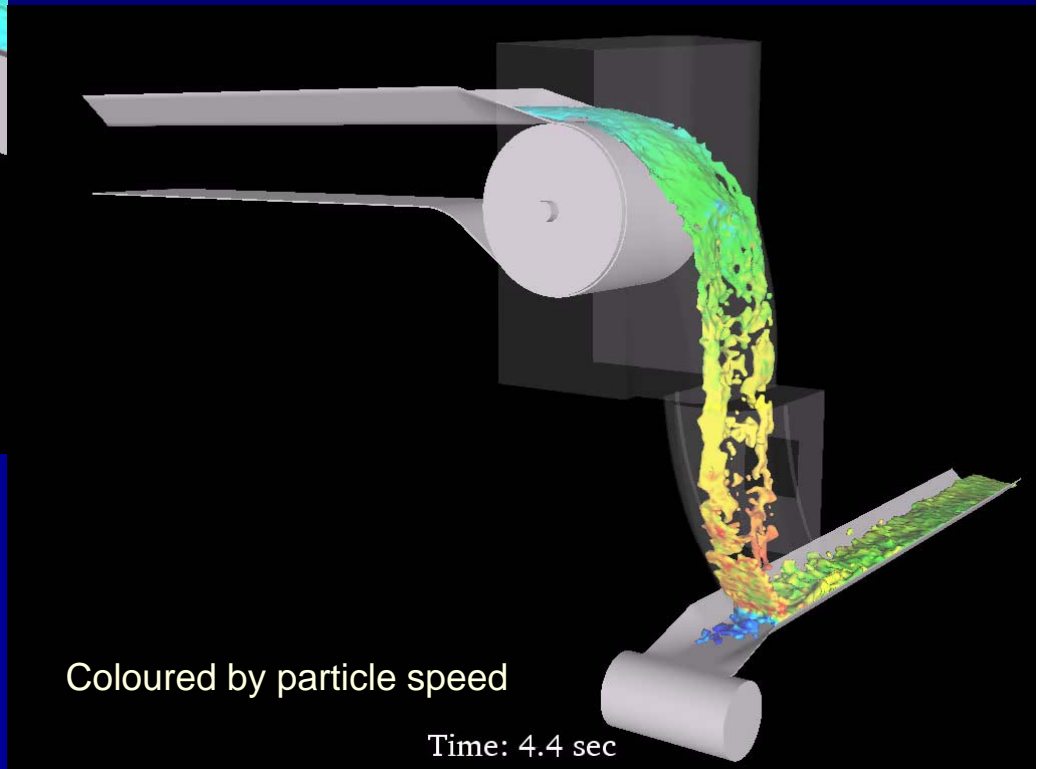


SPH is easily able to simulate this complex free surface flow

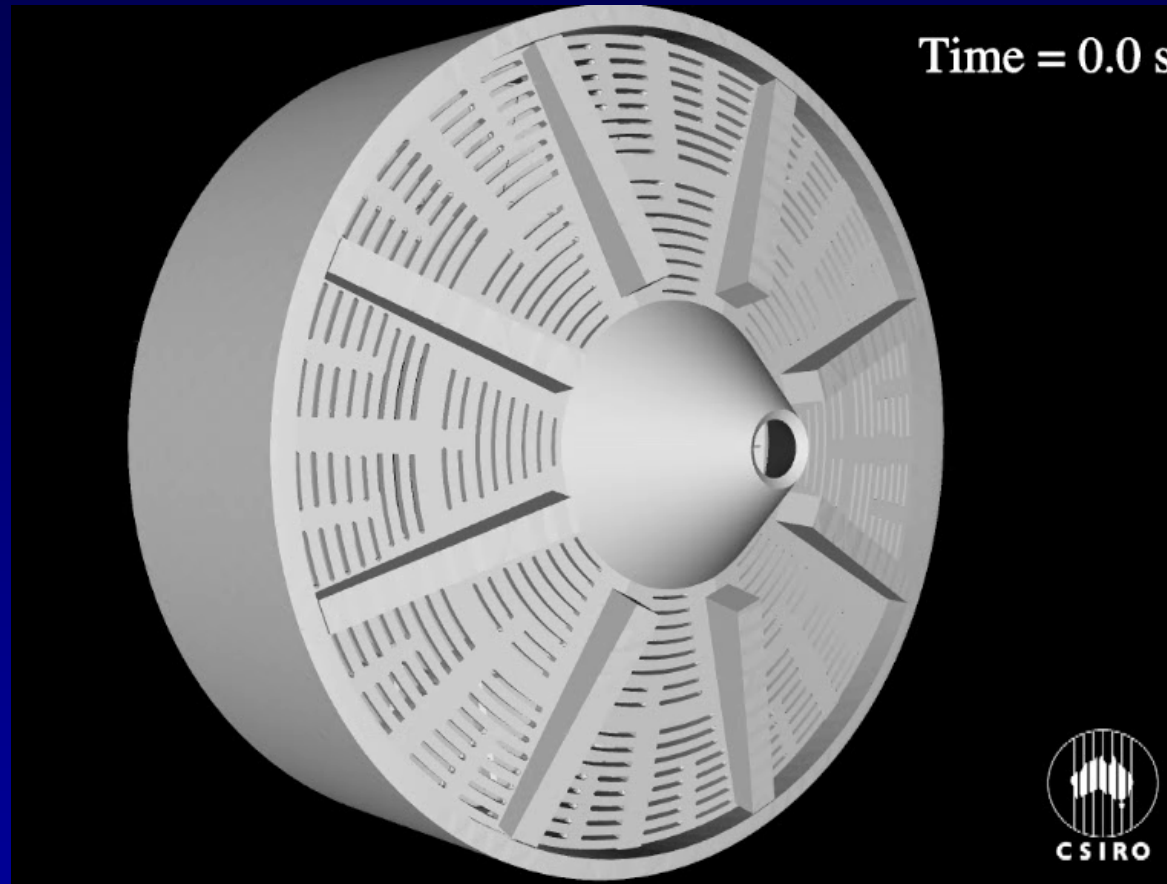
Next step is to add suitable material rheology

Interested in flow of fine material (eg. alumina) and high cohesive, sticky materials (eg. mud).

Both are best represented as a pseudo-fluid, so we use SPH to model these flows



Slurry discharge from a SAG mill

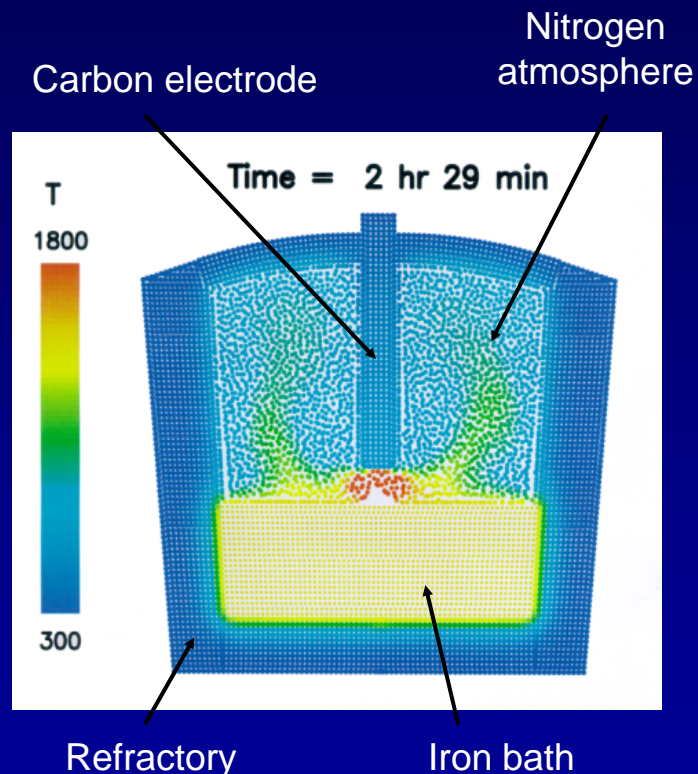


Slurry flows through the grate and is lifted by the radial pulp lifters, discharging at nearly vertical positions.

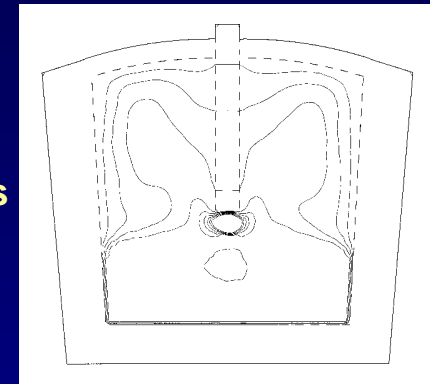
Pyrometallurgy

Electric Arc Furnace Modelling

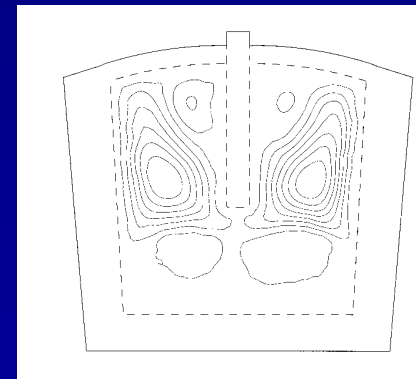
Heat and multi-material fluid flow is modelled in an electric arc furnace



Isotherms



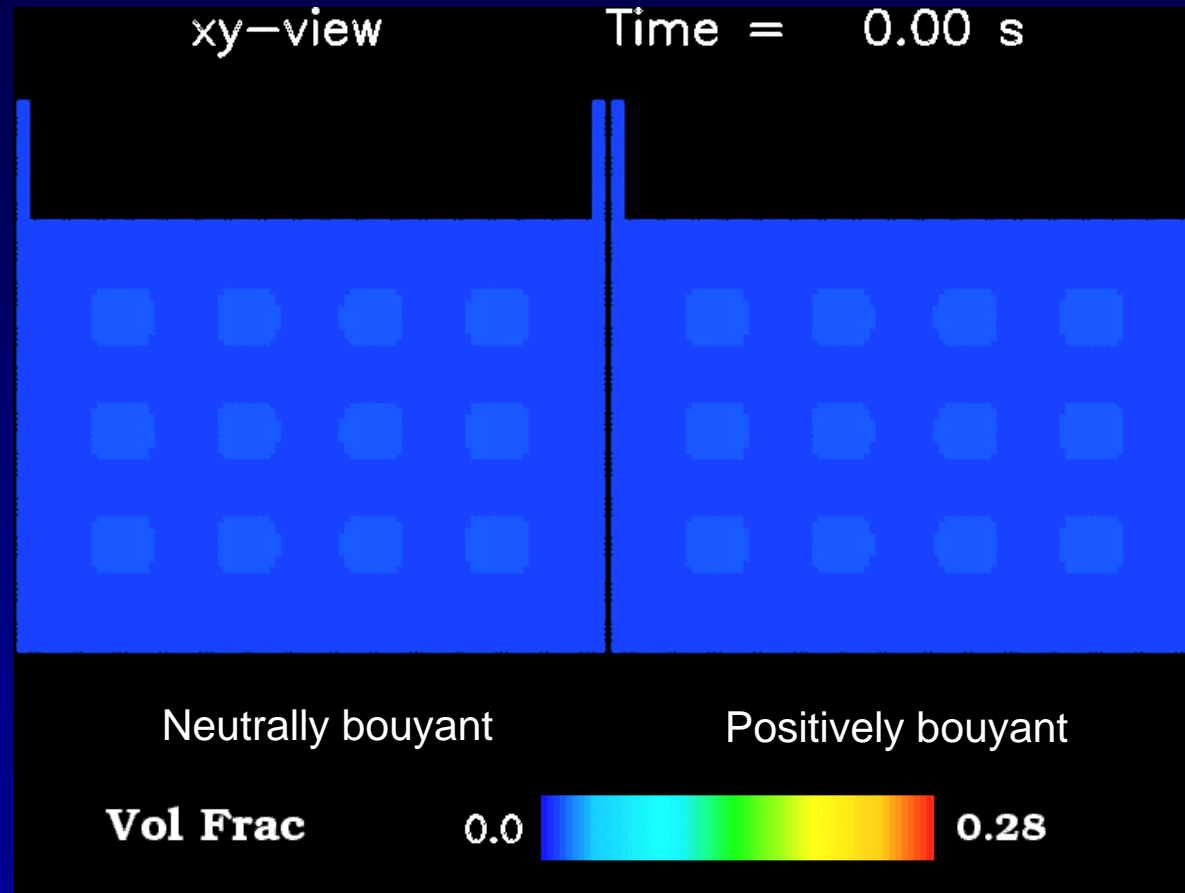
Liquid iron bath case



Streamlines

The heating phase of the furnace with a 60 kW arc from electrode to the bath

Gas-liquid-solid model in 2D



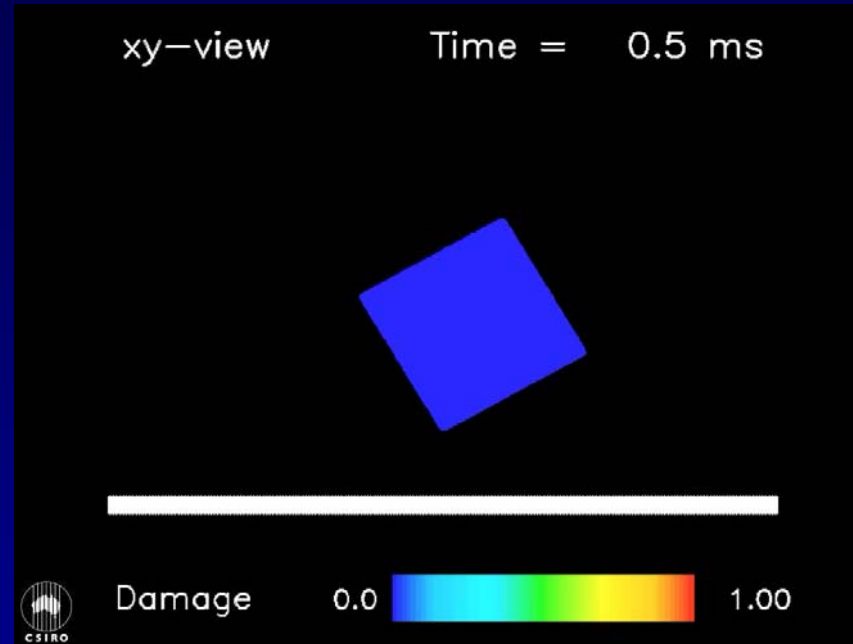
- Heat transfer controls reaction rates
- Reaction rates control gas generation
- Gas transport influences fluid and solid circulation

The fluid and pellets are colored by gas volume fraction

- Neutrally buoyant pellets move due to gas transport and central updraft
- Reaction rates and gas generation vary around the particulates with corners becoming hotter and generating coherent gas streams

Fracture

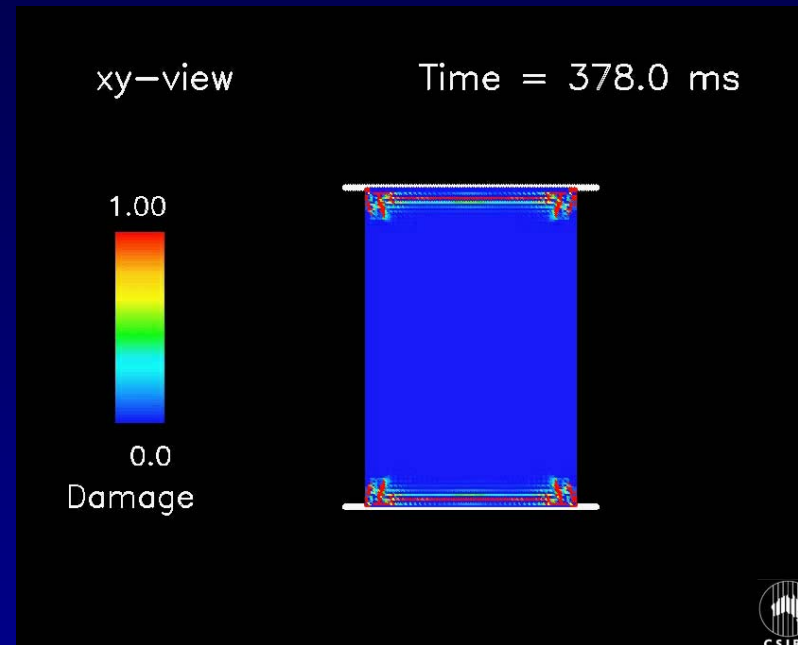
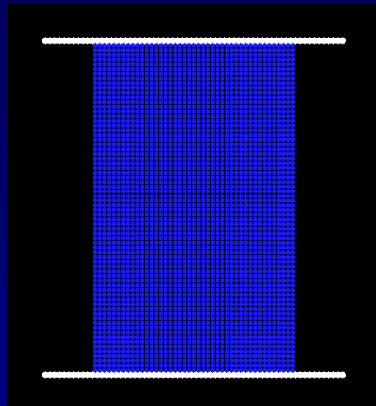
Impact fracture of a square rock



Impact Velocity
100 m/s

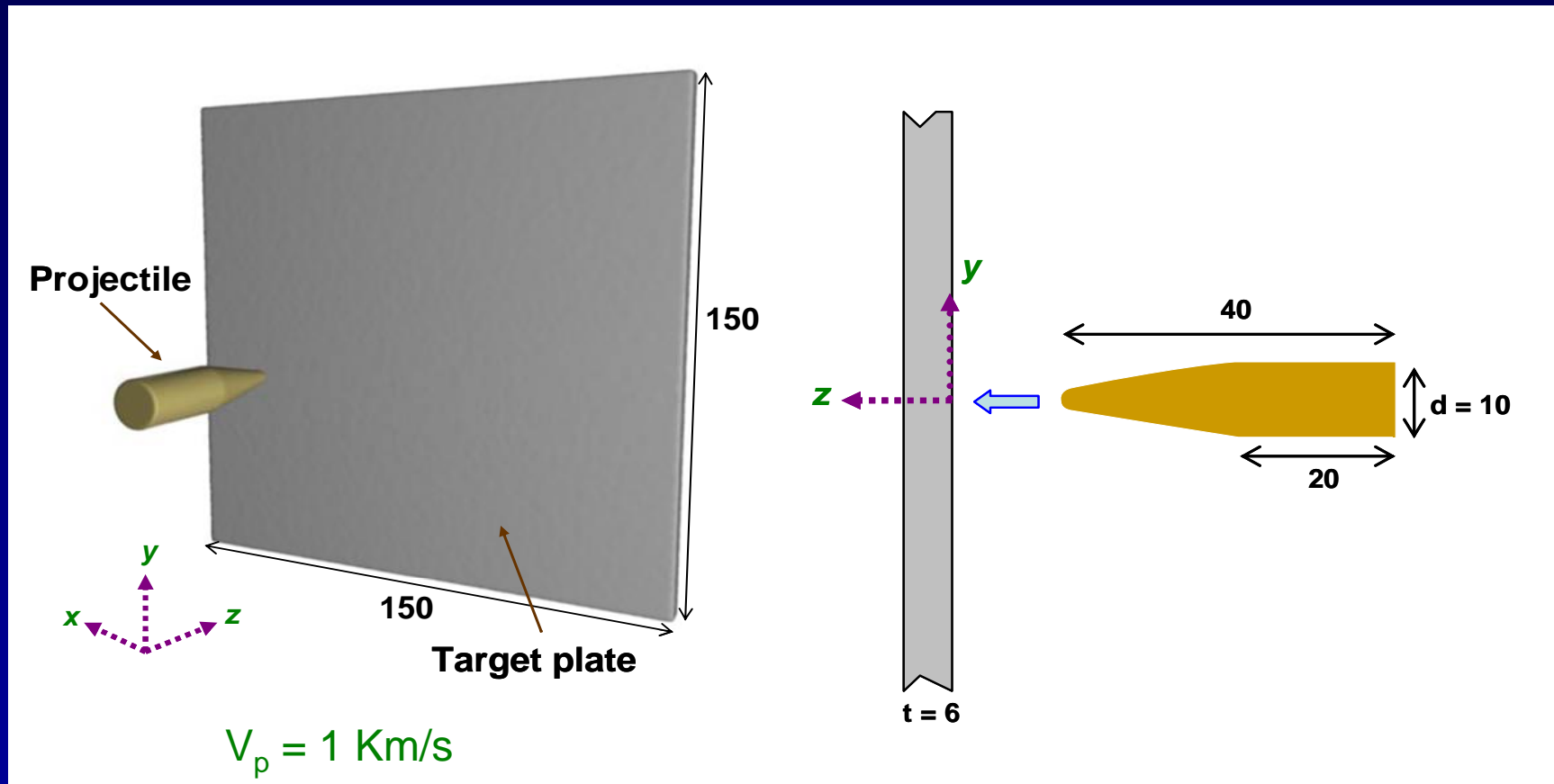
- Initial damage occurs at the impacting corner
- Damage then develops in the center of the block and along a diagonal path from the impact corner. Primary fragmentation occurs along this diagonal
- This is followed by secondary fragmentation including delamination along the top and bottom edges
- Fracture pattern is plausible

Fracture in Uniaxial Compression



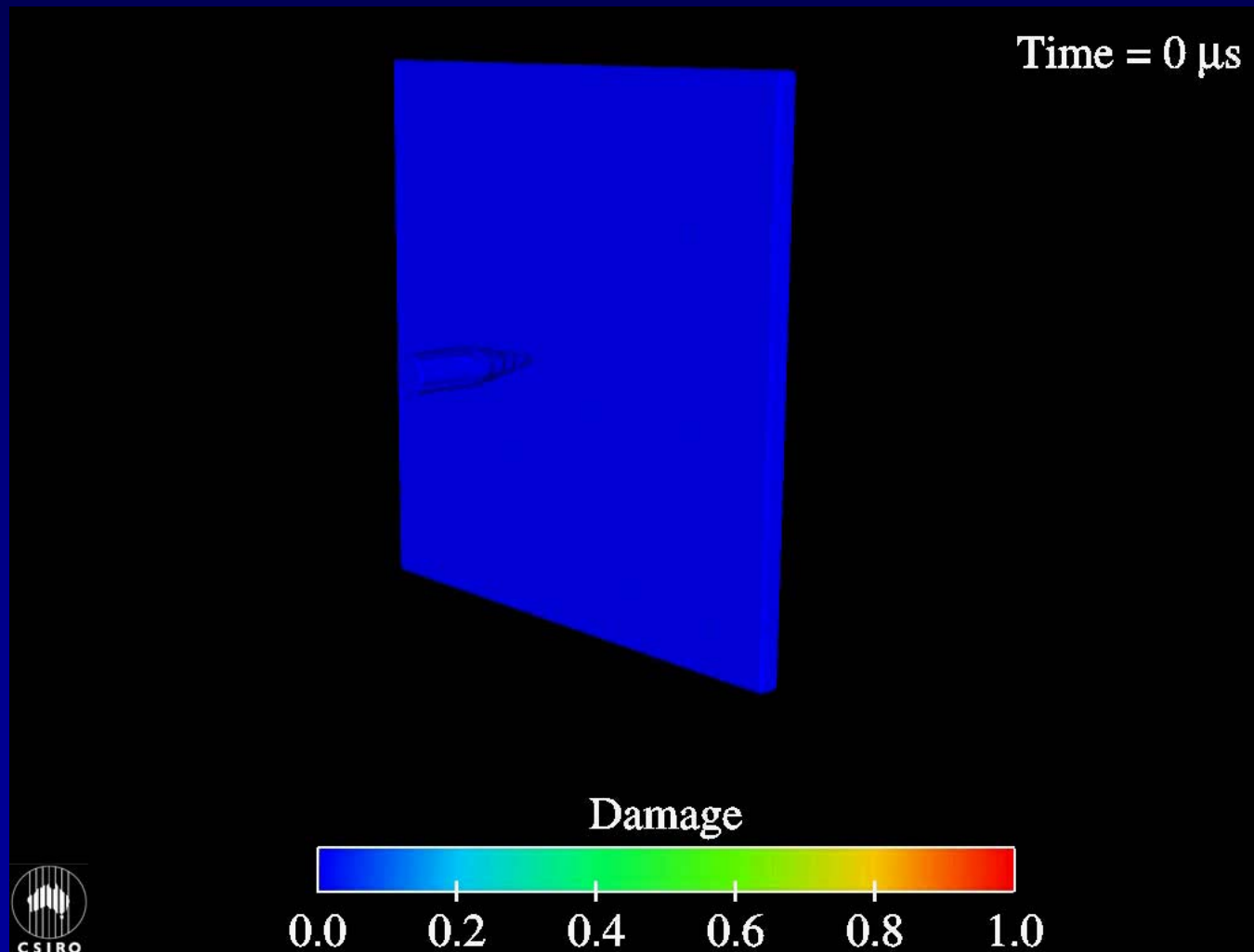
- Uniaxial compression generates lateral tension
- Early damage occurs near the loading pistons due to initial high stresses
- Damage propagates vertically from both ends and gradually weakens the specimen. Vertical fault lines appear
- Free edges aid in inhibit tensile stress growth so surface layers are not damaged, resulting in fracture parallel to but inside the edges

Hypervelocity Impact of a projectile onto a thin target plate



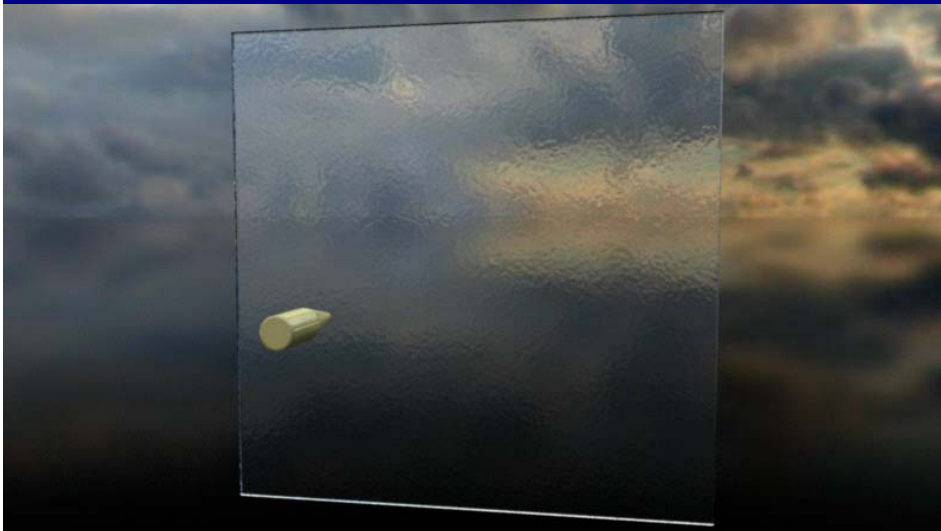
Collision configuration (all dimensions are in mm)

Dynamic crack propagation

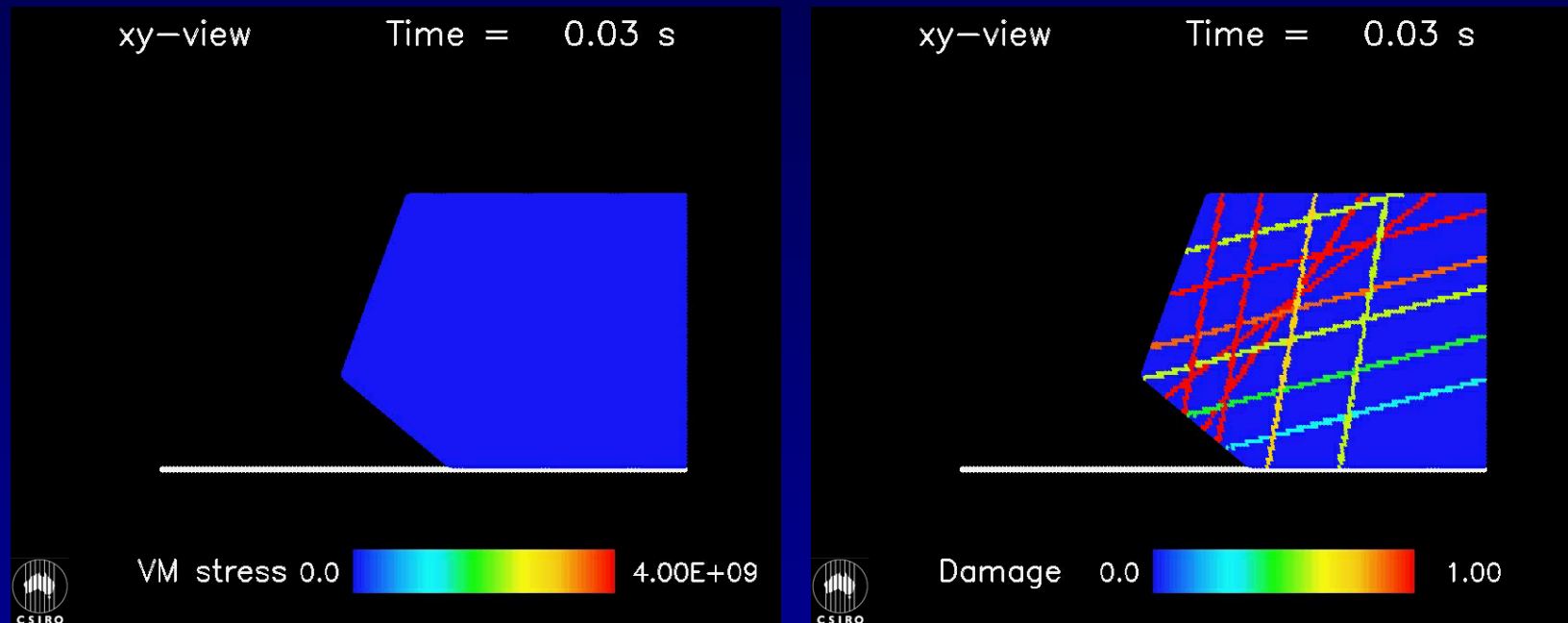


Breaking a Window

- SPH elastic solid
- Brittle damage
- Able to predict radial cracking
- Central pulverisation

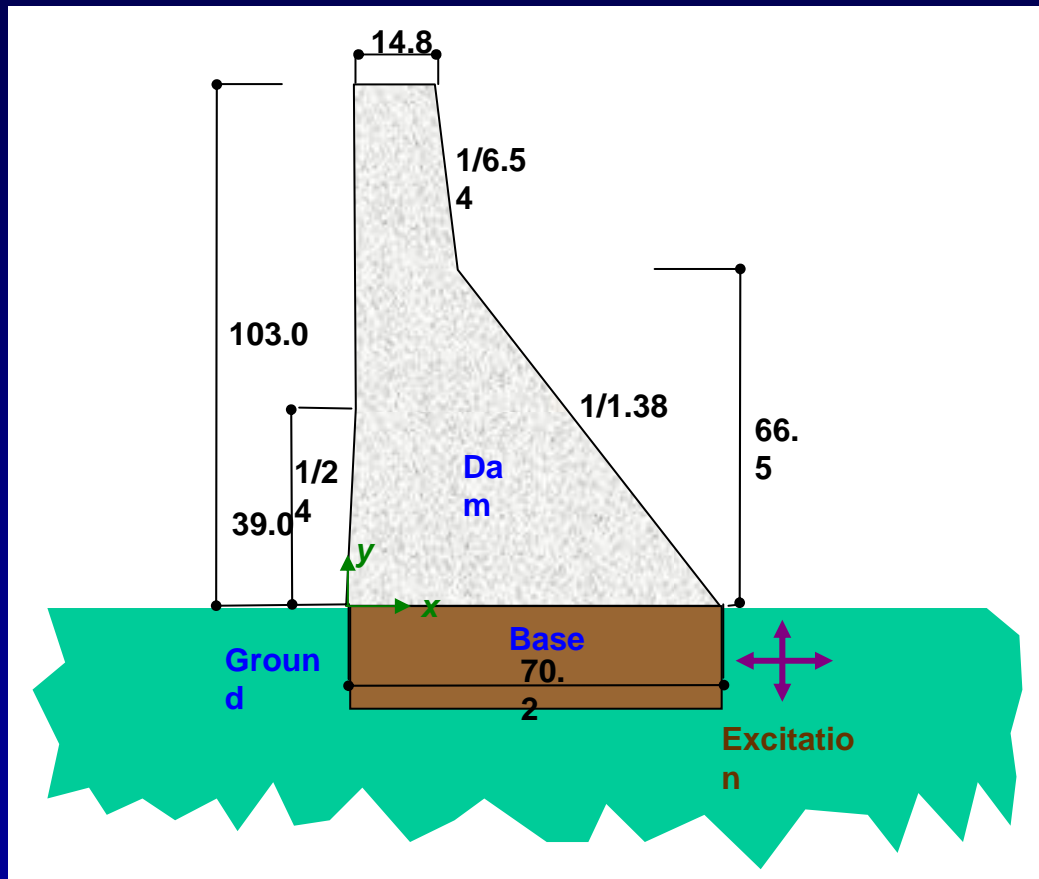


Fracture pattern in the rock



- Strata and rock joints are represented as bands with initial damage
- The damage modifies the transmission of stress and controls the subsequent fracture behaviour

Dam failure under earthquake load



Koyna dam

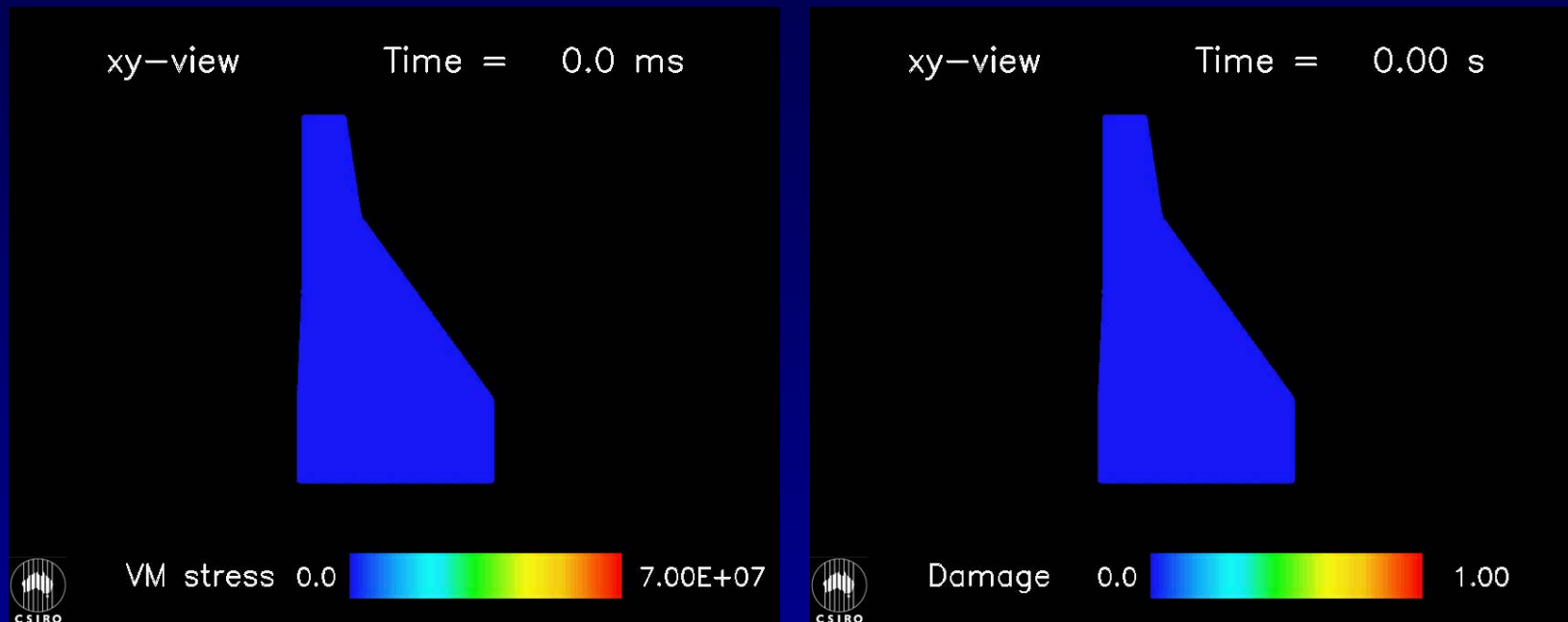
Dam wall: Concrete
Density = 2400 kg/m³
Bulk Mod. = 16.7 GPa
Shear Mod. = 8.1 GPa
Damage parameters:
 $k = 5.27 \times 10^{18}$, $m = 5.3$

Base: Basalt
Density = 2900 Kg/m³
Bulk Mod. = 58.3 GPa
Shear Mod. = 26.9 GPa

SPH discretisation:
particles = 5,856



Fracture pattern of dam



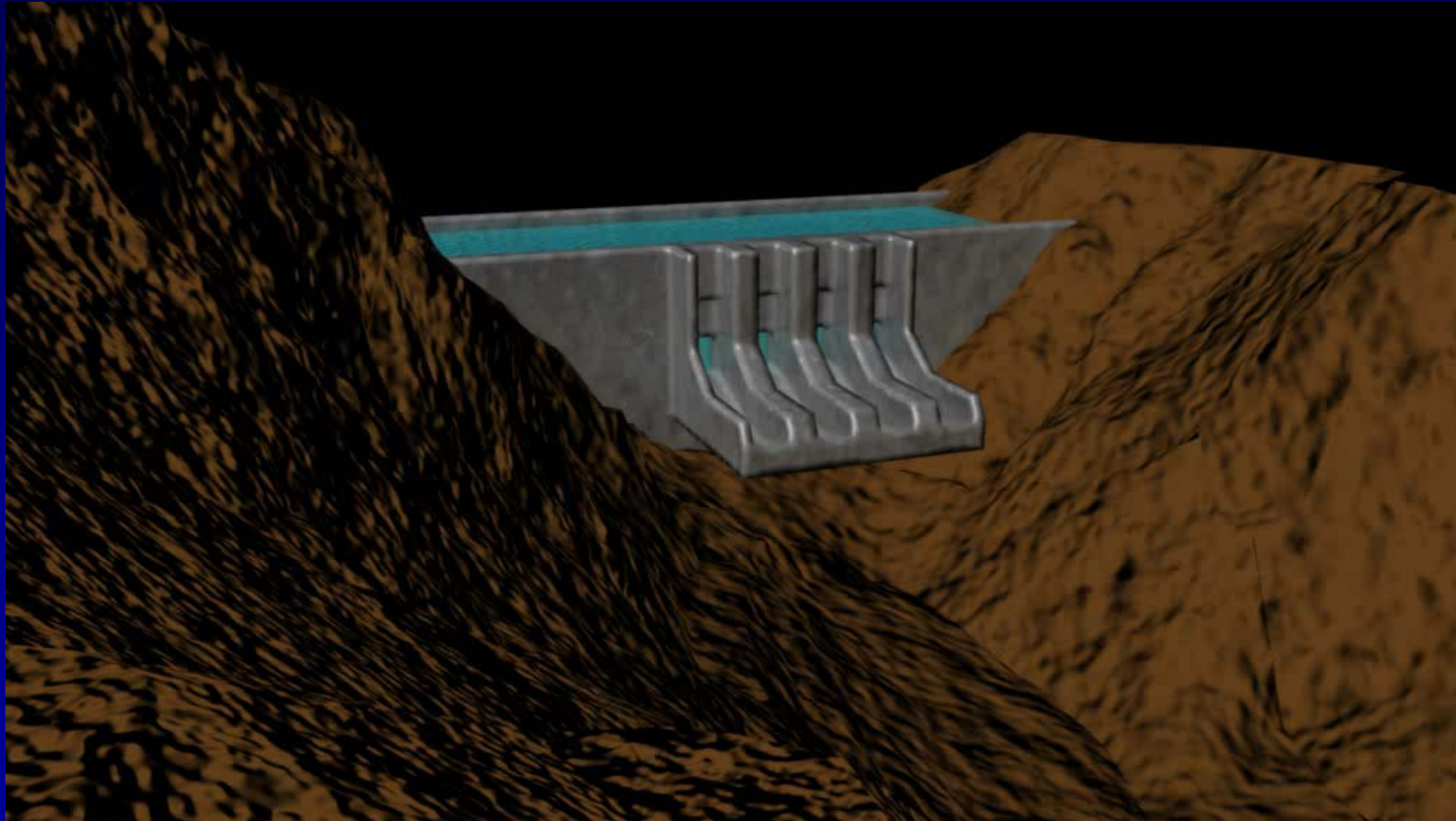
- Earthquake excitation of the ground under the dam wall
- Ground is elastic
- Concrete dam wall is brittle elastic
- Complex interaction of reflected waves within the structure lead to rapidly varying concentrations of stress that drive fracture behaviour

Geophysical and Civil Engineering Flows

Dam Break – Triunfo pass, Ca



Discharge from a spillway



Water discharges from a simulated scale model dam

St. Francis dam collapse



Fluid nodes = 1.7 million

Total nodes = 2.4 million

Fluid resolution = 4 m

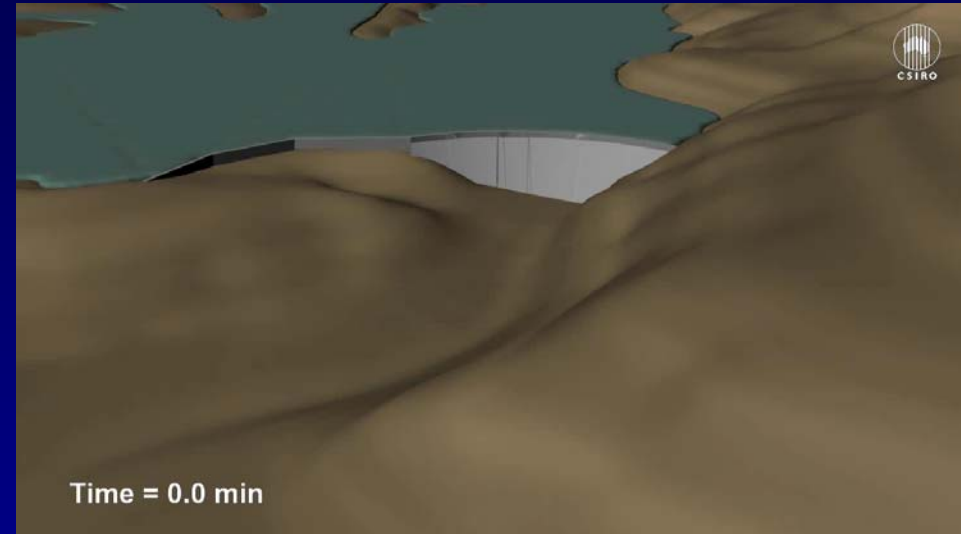
Resolution of topography = 8 m

CPU time = 3 weeks

Distance covered = 8 km

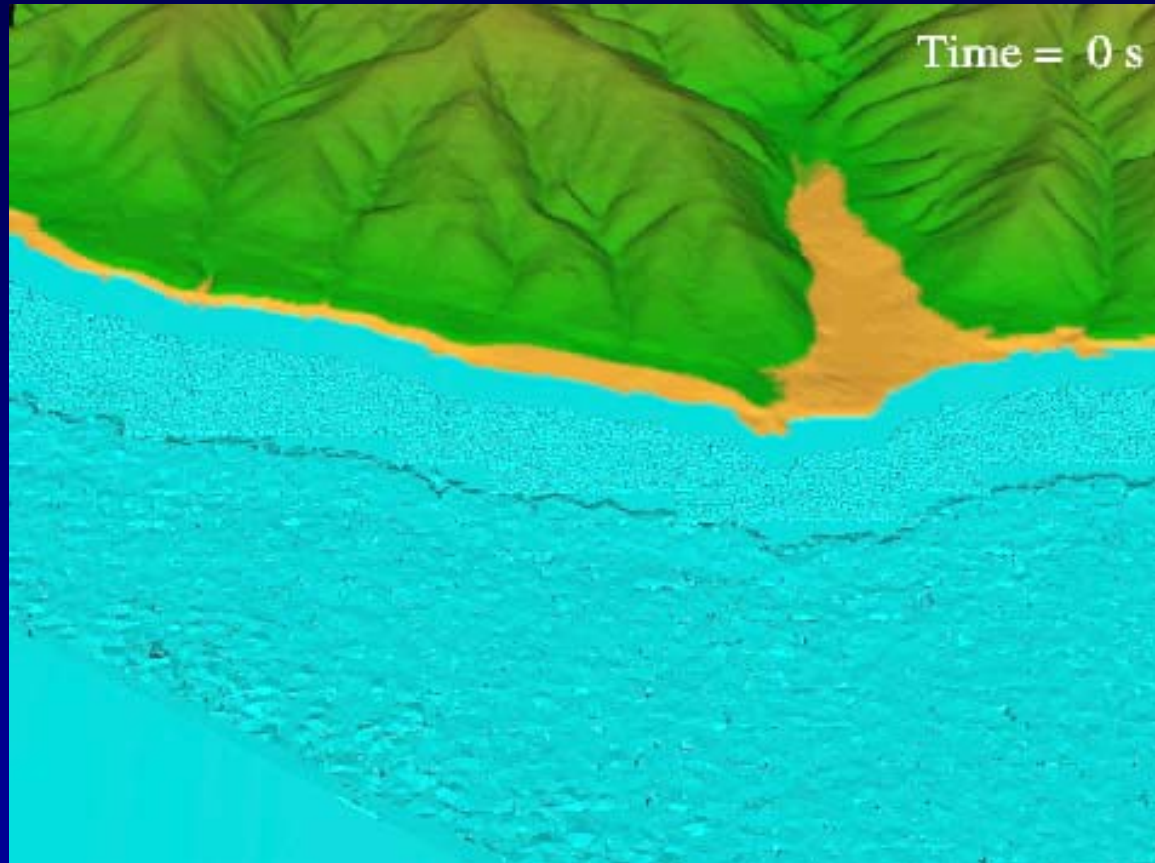


St. Francis dam collapse



- Nature of the dam wall failure affects the rate of water release and therefore the rate and pattern of inundation
- SPH can easily include the large solid dynamic objects such as sections of failed structures
- SPH can also be used for erosion and overtopping scenarios

Tsunami modelling



40 m high
wave moving
at 50 km/h
obliquely to
the shoreline

Allows assessment of the inundation patterns and risks from tsunamis and high tides. Also can examine the effect on structures such as oil rigs, ships, coastal defences and buildings.

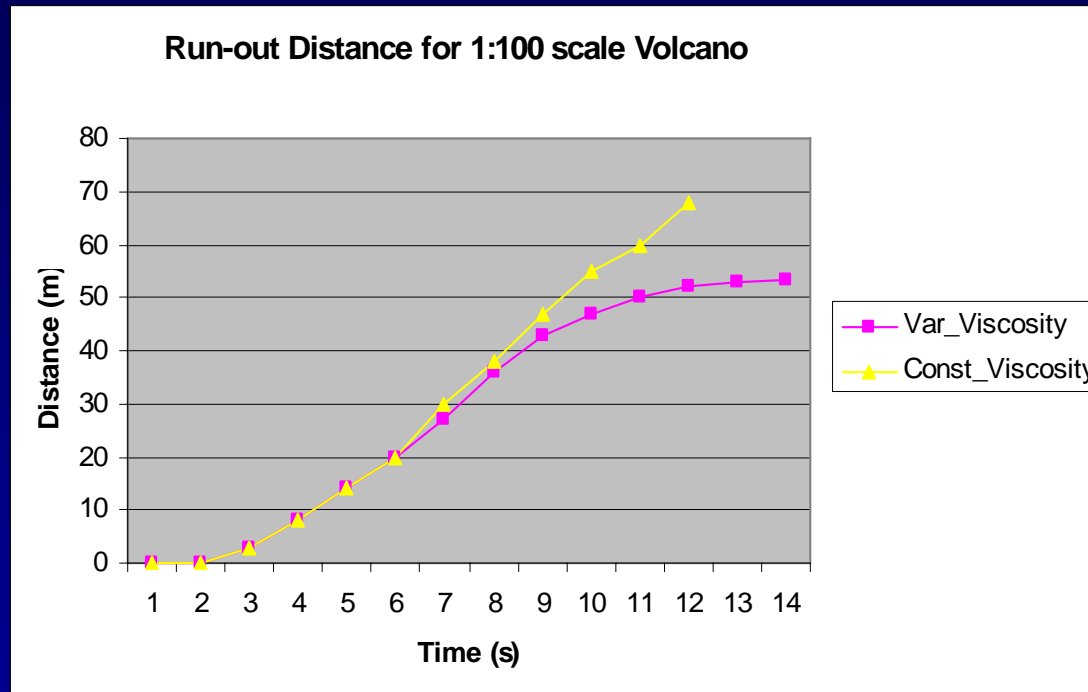
Volcanic Lava Flows



1:100 scaled
topography

2.6 m diameter lava jet located 60 m from the coastline

Effect of variable viscosity on run-out distance



Comparison between run-out distances predicted for constant and variable viscosity lava flows

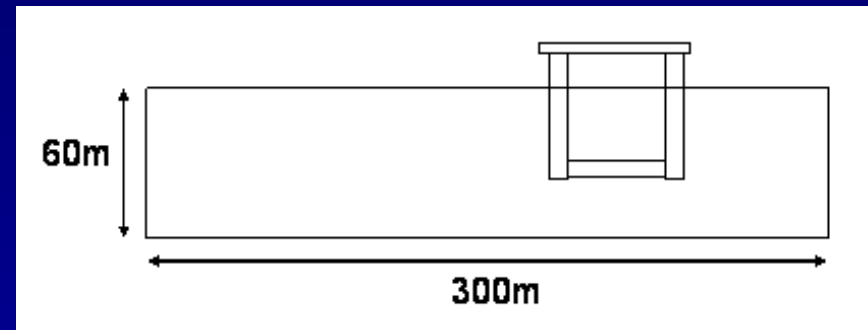
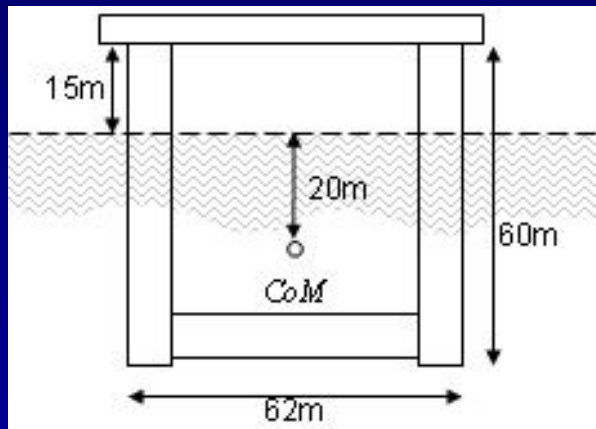
Offshore Wave - Structure

Moored floating oil platform

Floating platform could be fitted for production or drilling

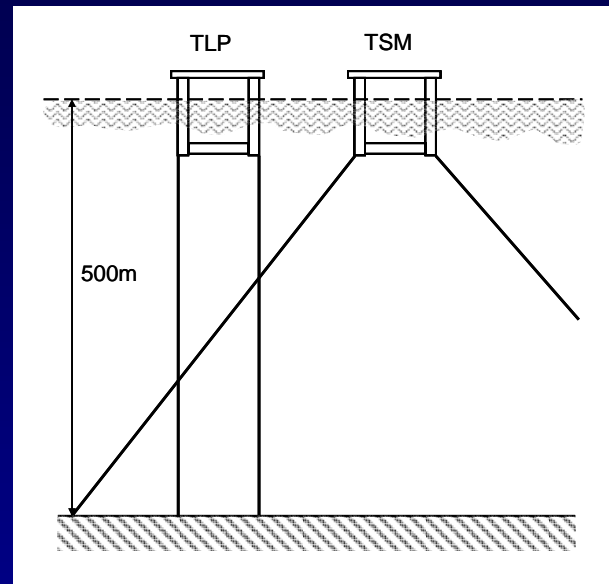
The width of fluid in the direction not displayed is 150 m. The domain is periodic in both spatial directions

The cables extend through the real water depth of 500 m



Waves of the desired height and shape are created using a force attractor in the space leading up to the floating rig. The waves are damped out rapidly once they pass through the end of the domain so that they do not reach the platform a second time

Mooring systems

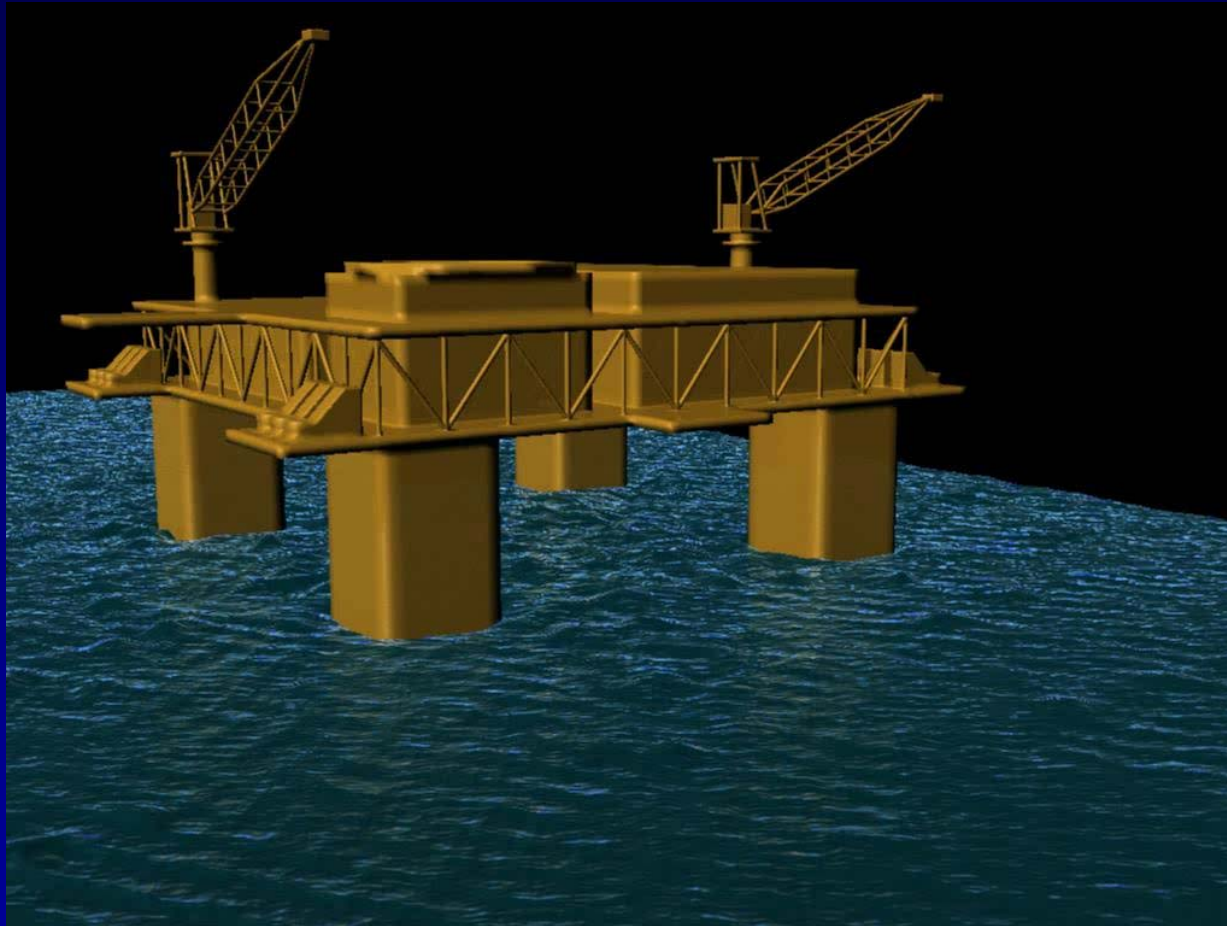


Four sets of vertical cables are attached to the outer bottom corners of the platform

- TLP – cables are vertical
- TSM – cables are directed down and outward at 45 degrees

Platform weight 32000 tonnes; Cable Young's modulus of 1.5×10^{11}

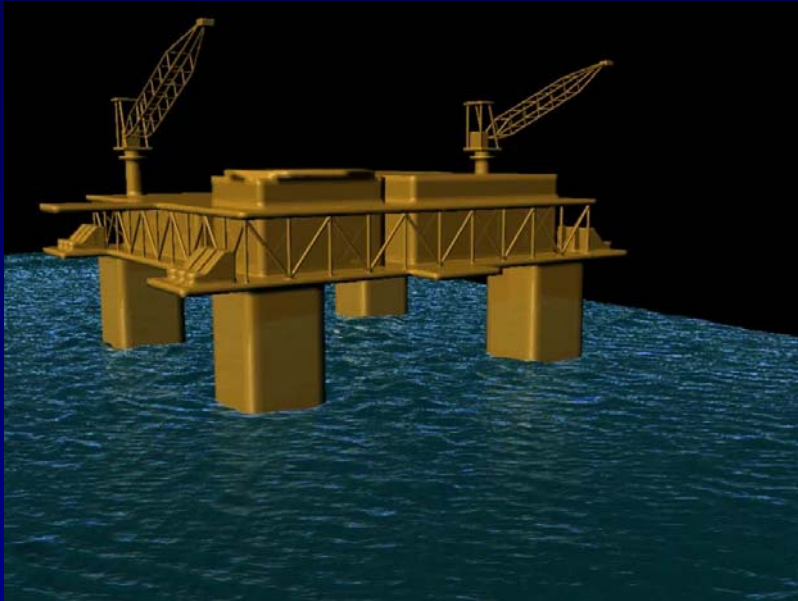
Oil rig – 11 m wave



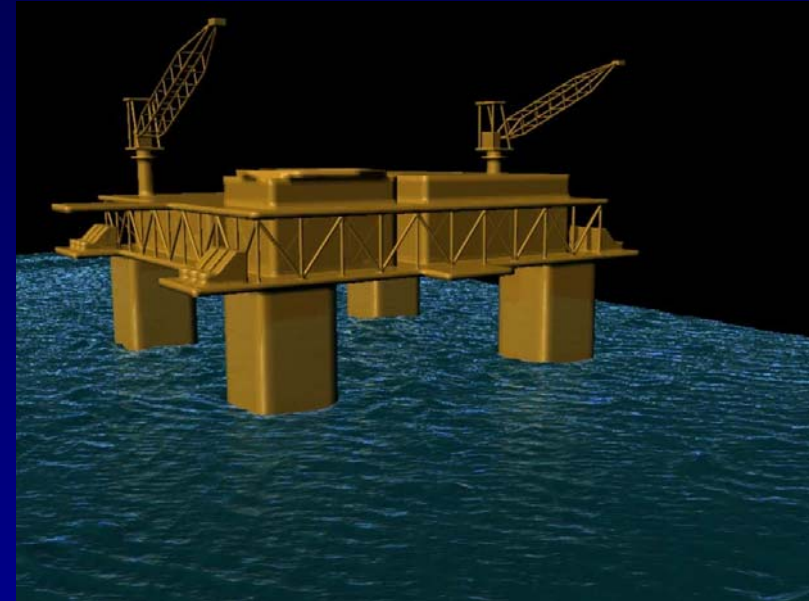
820,000 fluid particles, 200,000 nodes in the platform structure

45 hrs cpu per minute of simulation duration

Rogue wave impact



TLP

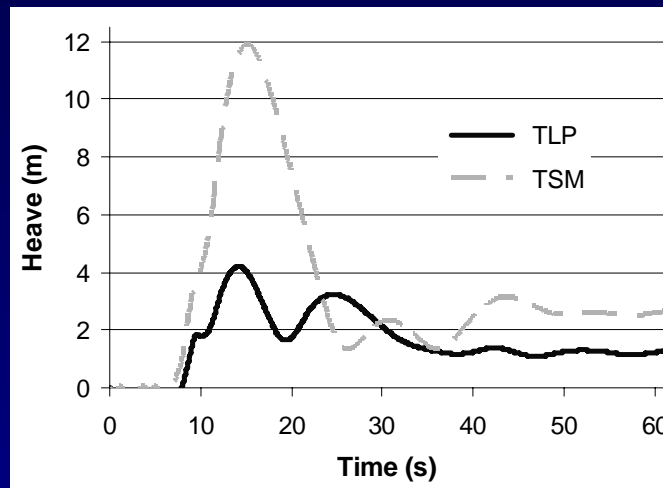
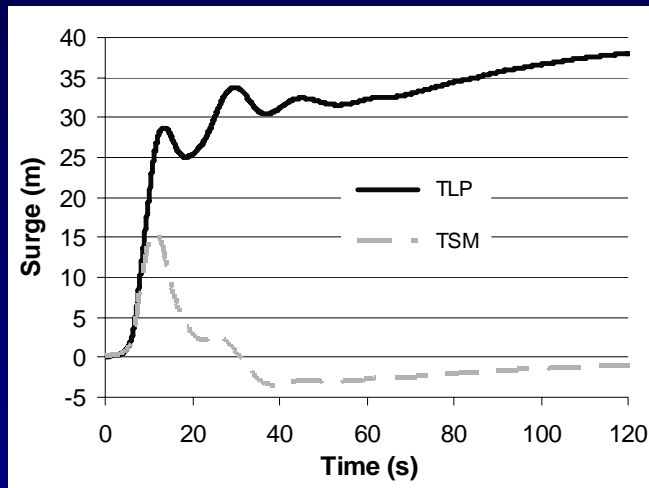


TSM

- The TLP platform tips over, partially submerges and surges, then floats back up and gradually straightens
- The TSM platform tips over, partially submerges but has lower surge. It rapidly straightens but then tips over again as the heave declines. There is then a complex interplay between surge, heave and pitch.

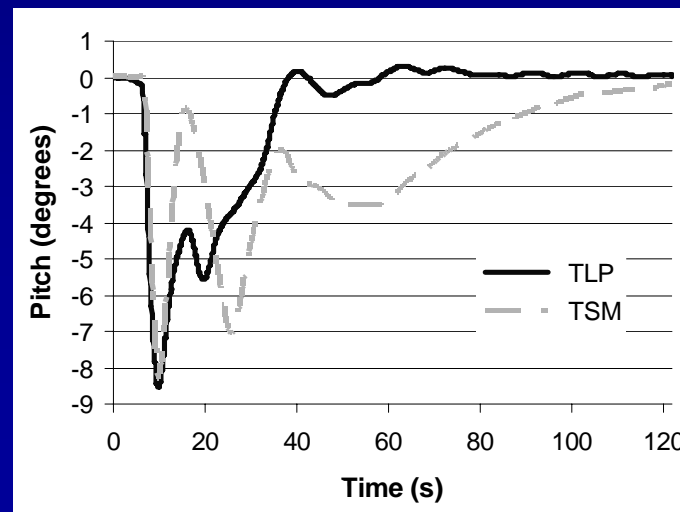
Rogue wave impact

Surge



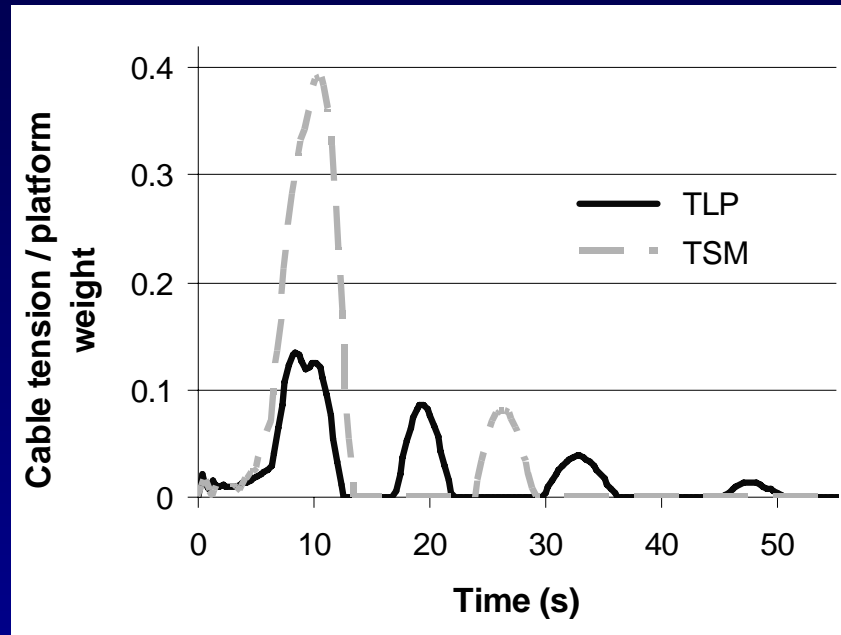
Heave

- TLP surge is much higher and recovery is very slow. Its motion is relatively simple
- TSM heave is much higher. As the heave declines it produces a second sharp increase in pitch. There is a complex coupling between all three d.o.f.



Pitch

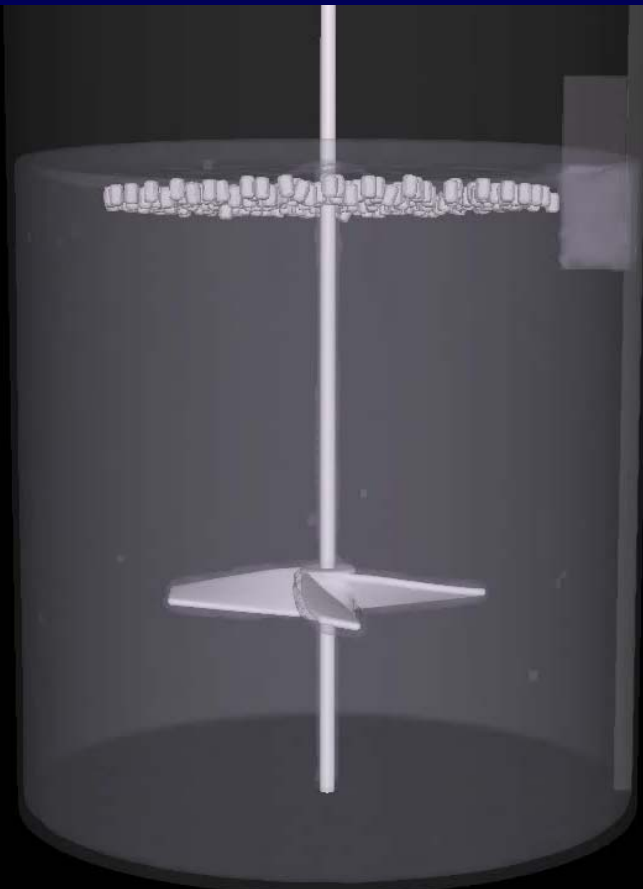
Rogue wave impact



- Tension in the TSM cables are around 3 x higher
- This is the force required to resist the high surge and prevent the platform moving substantially in the wave direction.
- The peak tension would exceed that required for breakage of the cables used here

Particulate – Fluid simulation

Mixing of particulates in fluid



Time: 0.0 sec

Impeller speed 200 rpm

Solids loading 1.5 kg

Tank diameter 1 m

Particulate diameter = 16 mm

Particulate length = 25 mm

At high speed the recirculatory flow in the mixing tank is able to suck down the highly bouyant pellets

Bubble – Fluid simulation

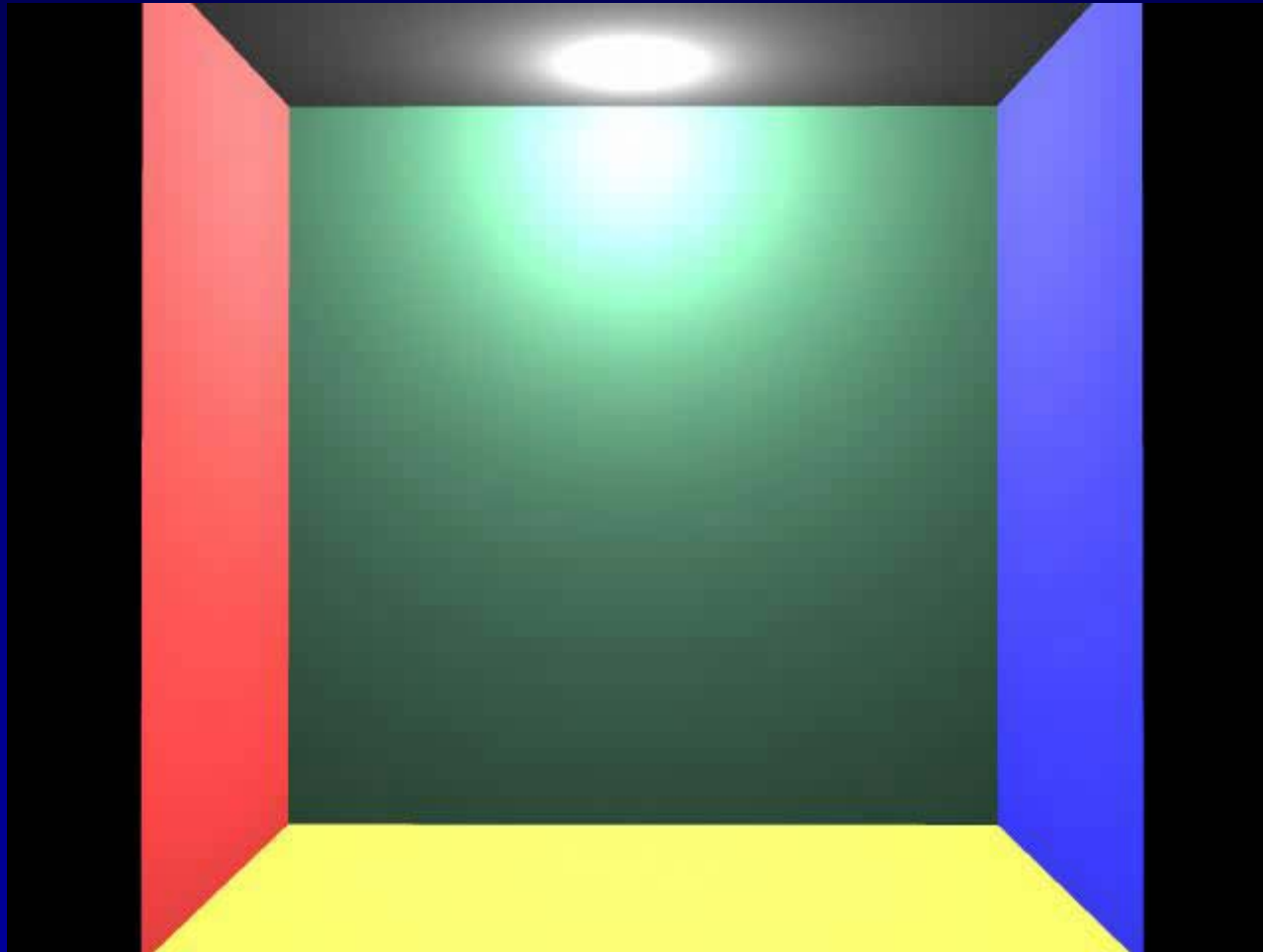
Discrete bubbles and foam

Continuous phase representations of gas and bubbles cannot capture bubble scale physics, such as predicting bubble-bubble interactions, bubble-particulate collision and foam behaviour.

For these systems discrete representations of bubbles are useful

- Small bubbles are represented as discrete spheres
- Bubbles are generated at nucleation sites on surfaces or from emitters
- Bubbles are coupled to the fluid via a drag term.
- Bubbles collide with each other and with solid bodies
- Coalescence and splitting is accommodated

Bubble motion in fluid

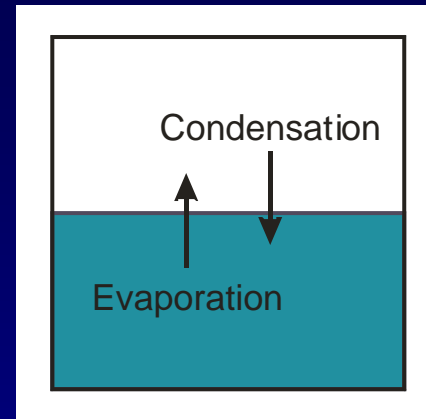


Coupled FD/FV - SPH

SPH-vapour coupling

Vaporisation is driven by:

- Temperature
- Vapour saturation
- Interface surface Area



Gas phase

Liquid phase

The net evaporation rate is the difference between the condensing and evaporating fluxes. This gives the Hertz-Knudsen relation:

$$\frac{\partial \rho}{\partial t} = \frac{\alpha}{L} \sqrt{\frac{m_p}{2\pi k_b T}} \left[p^* - \rho \frac{k_b T}{m_p} \right]$$

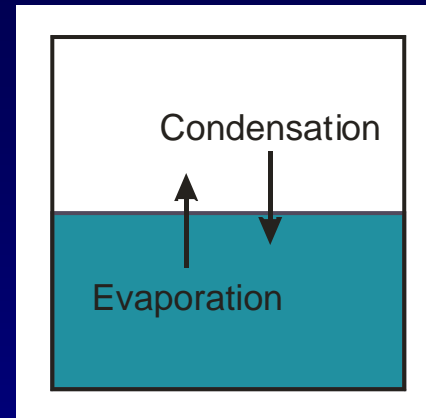
Where the vapour density is ρ , and the gas phase is assumed an ideal gas

Where sticking coefficient $\alpha \sim 0.1$, cell length scale L , mass of vapour molecule m_p , temperature T and vapour partial pressure p^ .*

SPH-vapour coupling

Vaporisation is driven by:

- Temperature
- Vapour saturation
- Interface surface Area



Gas phase

Liquid phase

The net evaporation rate is the difference between the condensing and evaporating fluxes. This gives the Hertz-Knudsen relation:

$$\frac{\partial \rho}{\partial t} = \frac{\alpha}{L} \sqrt{\frac{m_p}{2\pi k_b T}} \left[p^* - \rho \frac{k_b T}{m_p} \right]$$

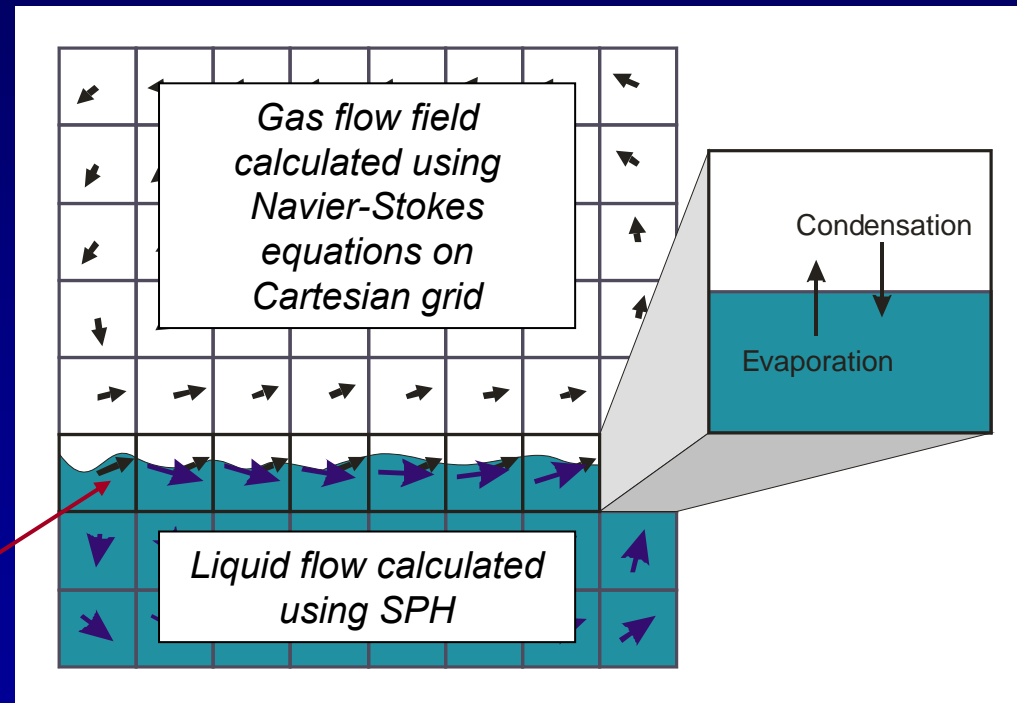
Where the vapour density is ρ , and the gas phase is assumed an ideal gas

Where sticking coefficient $\alpha \sim 0.1$, cell length scale L , mass of vapour molecule m_p , temperature T and vapour partial pressure p^ .*

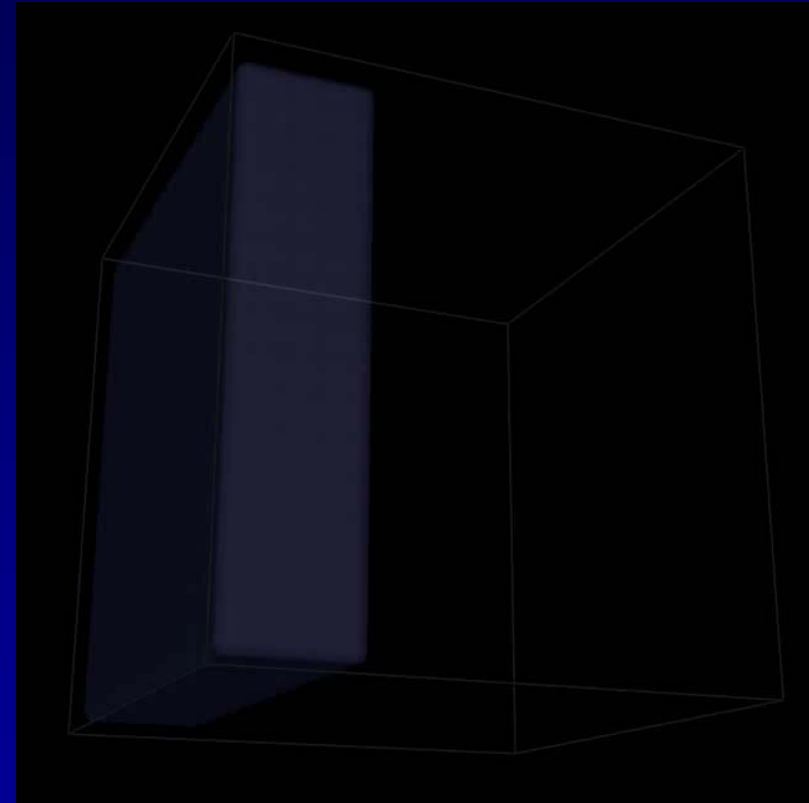
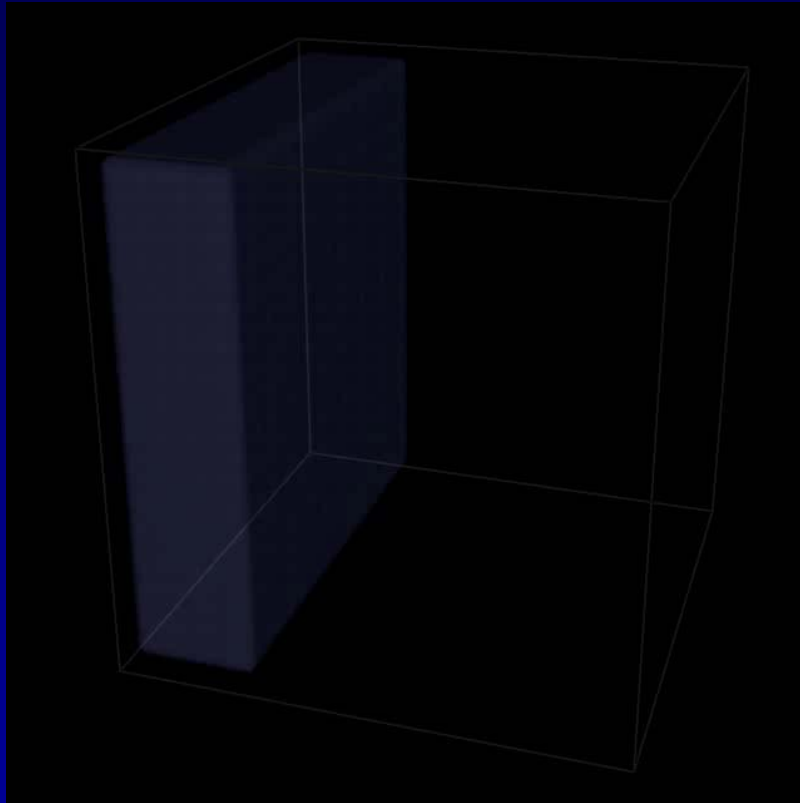
SPH-vapour coupling

- SPH and finite difference code coupled
- Vapour density passively advected
- Hertz-Knudsen relation used to update vapour density in interface cells
- Vapour diffusion included using Fick's law

SPH particles give immersed boundary at interface



Gas-fluid flow with vapour



Beach waves



Beer



Smoke



Flash flood



Digital water in real video



SUV through a flood



Flooding of a Cathedral

